CANADIAN THESES

THÈSES CANADIENNES

NOTICE

The quality of this microfiche is heavily dependent upon the quality of the original thesis submitted for microfilming. Every effort has been made to ensure the highest quality of reproduction possible.

If pages are missing, contact the university which granted the degree.

Some pages may have indistinct print especially if the original pages were typed with a poor typewriter ribbon or if the university sent us an inferior photocopy.

Previously copyrighted materials (journal articles, published tests, etc.) are not filmed.

Reproduction in full or in part of this film is governed by the Canadian Copyright Act, R.S.C. 1970, c. C-30.

AVIS

La qualité de cette microfiche dépend grandement de la qualité de la thèse soumise au microfilmage. Nous avons tout fait pour assurer une qualité supérieure de reproduction.

S'il manque des pages, veuillez communiquer avec l'université qui a conféré le grade.

La qualité d'impression de certaines pages peut laisser à désirer, surtout si les pages originales ont été dactylographiées à l'aide d'un ruban usé ou si l'université nous a fait parvenir une photocopie de qualité inférieure.

Les documents qui font déjà l'objet d'un droit d'auteur (articles de revue, examens publiés, etc.) ne sont pas microfilmés.

La reproduction, même partielle, de ce microfilm est soumise à la Loi canadienne sur le droit d'auteur, SRC 1970, c. C-30.

THIS DISSERTATION HAS BEEN MICROFILMED EXACTLY AS RECEIVED

LA THÈSE A ÉTÉ MICROFILMÉE TELLE QUE NOUS L'AVONS REÇUE

A Study of the Self-Trapped Exciton in Alkaline-Earth Fluorides

by

MICHAEL R. ADAIR

Thesis submitted to the School of Graduate Studies
of the University of Ottawa in partial fulfillment
of the requirements for the degree
of Master of Science in Physics

Physics Department
Faculty of Science
University of Ottawa
Ottawa, Canada
1986

ISBN 0-315-36467-X

UNIVERSITÉ D'OTTAWA
UNIVERSITY OF OTTAWA

Abstract

The structure of the self-trapped exciton (STE) in CaF_2 and SrF_2 is studied within the framework of the one-electron Hartree-Fock approximation. The equilibrium configuration of the crystal containing an excited electron and a self-trapped hole is determined by minimizing the total energy of the system with respect to the positions of the ions surrounding and including the hole center and the excited electron wavefunction. The electron is represented by a linear combination of floating 1*s* gaussians. We use a hybrid pseudopotential method to determine the energy and states of the defect electron. Pair-potentials of the Born-Mayer form are used to represent the lattice. The polarization energy is included through a first order Mott-Littleton treatment. The electron wavefunction and lattice relaxation are determined in a self-consistent way. We found that the equilibrium configuration of the STE resembles a nearest or next-nearest neighbour pair of F and H centers, rather than a $(V_k + e^-)$ configuration. Moreover, the F-H center pair is formed spontaneously upon the capture of an electron by a V_k center. The H center may be found in any one of three possible configurations, in complete agreement with experiment. We calculate the absorption spectrum at equilibrium and find this to have slightly higher energies than observed. We also show that the adiabatic potential barriers for the conversion of the F-H pair from one orientation to another to be very small. This gives a good probability for this process to occur as observed experimentally.

Acknowledgments

First of all, I would like to thank Dr. K.S. Song for all of his help, encouragement and support over the past two years. I feel privileged to have had this opportunity to have worked with him and it has been both stimulating and enjoyable to do so.

I would also like to thank Dr. C.H. Leung for his patience and tutoring which has made this work that much easier to complete.

Thanks must also go to my family and friends for their support and encouragement. Last and certainly not least, I would like to thank Sandra, to whom I dedicate this work, for her patience and support.

Contents

CHAPTER I - *Introduction*

In this thesis, we shall present a study on the structure of the self-trapped exciton in alkaline earth fluoride crystals. We shall restrict our attention to the CaF_2 and SrF_2 crystals although similar effects appear in BaF_2.

We begin by describing the fluorite crystal structure as shown in Figure 1. It is composed of an FCC sublattice with a basis of three ions, anions at $(\frac{1}{4},\frac{1}{4},\frac{1}{4})$ and $(\frac{3}{4},\frac{3}{4},\frac{3}{4})$, and a cation at (0,0,0). This means that each anion is surrounded tetrahedrally by the cations. The anions form an octahedral arrangement about the body-centered interstitial site which is alternately occupied by a cation or is empty. The lattice constant, a_0, is 10.3 (a.u.) in CaF_2 and 11.6 (a.u.) in SrF_2 .

The fluorite crystals we study have a direct band gap. The gap width, 12.2 eV in CaF_2 and 11.44 eV in SrF_2 [1], classify these materials as insulators. The first exciton peak appears just below the conduction band edge at 11.18 eV in CaF_2 and 10.6 eV in SrF_2 . The valence band arises from the $2p$ orbitals of F^- while the conduction band at the minimum comes from the $4s$ orbitals of Ca^{2+} in CaF_2 and from the $5s$ orbitals of Sr^{2+} in SrF_2 . The crystal bonding is strongly ionic in character[1].

Next, we shall briefly describe some of the nomenclature associated with point defects which we shall frequently use. A V_k center consists of a diatomic halogen molecule, F_2^-, in a lattice. It is also often refered to as a self-trapped hole. It is formed by a covalent bond between two nearest neighbour anions which have lost an electron (or alternatively, trapped a hole). It is usually detected by electron paramagnetic resonance (EPR) measurements of its unpaired spin, or by optical excitations of the hole. The V_k center in fluorites is

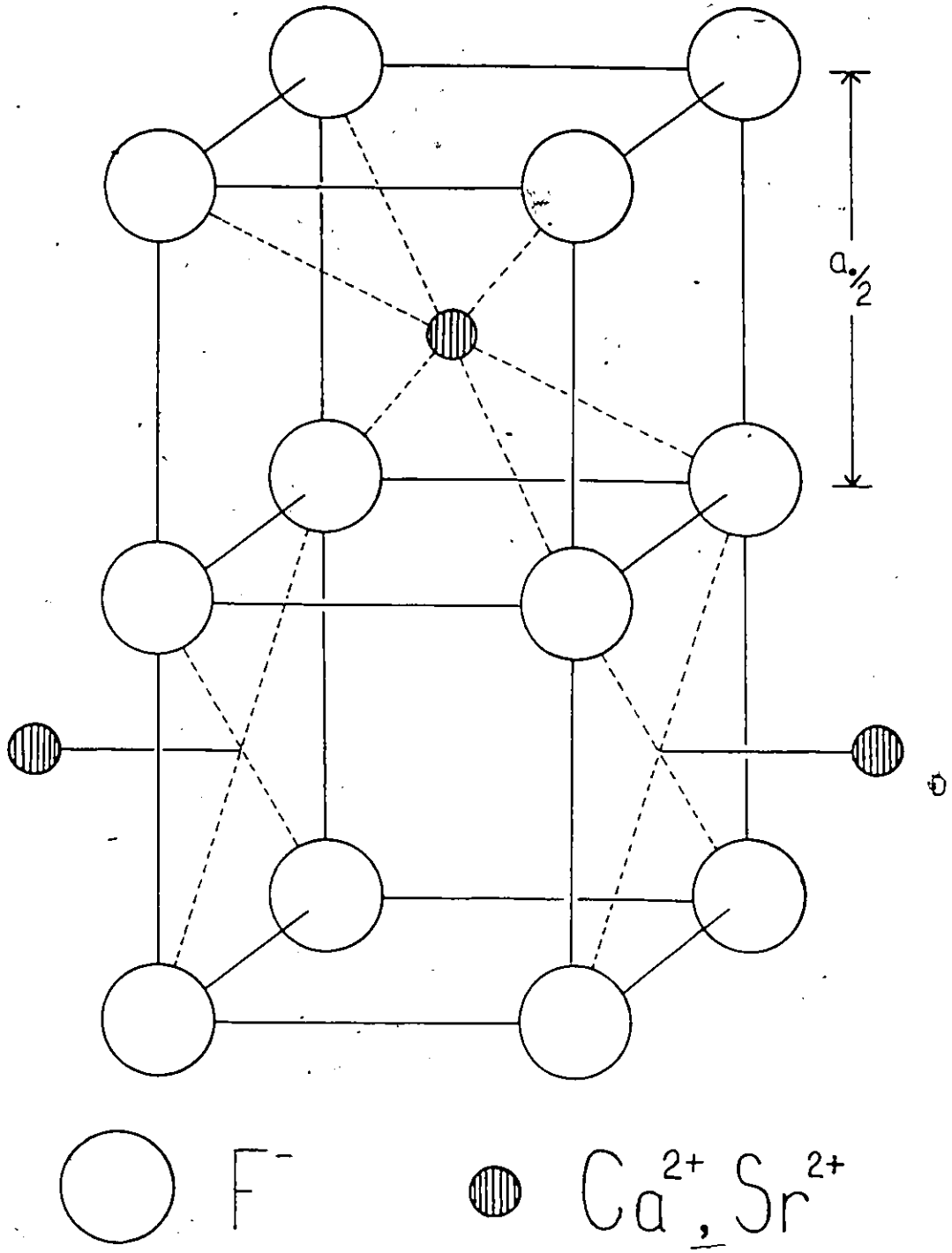

Figure 1
Fluorite crystal structure

aligned along a $\langle 100 \rangle$ cube axis[2].

We shall use the "molecule in a lattice" model to describe the V_k center. This model suggests that the properties of a free F_2^- molecule remain largely unchanged in the midst of a lattice. This assumption has shown to be a valid approximation by a number of authors[3,4,5] due to the strong covalent bond of the two halide ions.

We shall also be concerned with H centers. An H center is a hole trapped on an interstitial anion. In the case of the fluorite crystals, it is comprised of the diatomic halogen molecule with one ion at a substitutional anion site and the other ion near an empty body centered interstitial site. It has been established by EPR techniques that the H center lies along a $\langle 111 \rangle$ axis in the fluorite crystal[2].

Another defect we shall refer to is the well known F center. This consists of a neutral anion vacancy, in other words, an electron trapped at an F^- vacancy. The properties of F centers have been extensively studied using EPR and optical techniques[1].

These defects are known collectively as colour centers because of their strong absorption and luminescence bands in the visible region of the spectrum.

The self-trapped exciton (STE) was first detected in alkaline earth fluorides by Beaumont *et al*[2]. Properly defined, the STE is a self-trapped electron bound to a V_k center or self-trapped hole. This is shown schematically in Figure 2(a). However in the alkaline earth fluorides, the STE has never been observed in this configuration and it has been shown to more closely resemble a nearest or next-nearest neighbour F and H center pair[6] as shown in Figures 2(b)-2(e).

The STE in alkaline earth fluorides closely parallels the STE in alkali halides. In the

alkali halides, the V_k center is aligned along a $\langle 1\bar{1}0 \rangle$ close-packed direction. The STE has long been accepted as a $(V_k + e^-)$ system[15] despite some serious problems. Recently, Leung, Brunet and Song[8] have performed a self-consistent calculation along the lines adopted in this thesis and have established that the STE in alkali halides is strongly off-centered. The STE is more like a nearest neighbour F-H pair and many of the difficulties previously unaccounted for are now satisfactorily explained.

The usual method for producing colour centers in fluorites is with ionizing radiation, either X or β rays. The incoming photon removes an electron from an anion, after which the unpaired electron becomes shared by a pair of nearest neighbour anions forming a V_k center. The excited electron is then attracted back to the hole center. The electronic configuration of the $(V_k + e^-)$ is split into a singlet and a triplet state by the exchange interaction. The singlet states recombine rapidly with a lifetime of $\sim$ 10 nsec[10]. There are three other decay components in the recombination emission spectrum with considerably larger lifetimes originating from the triplet states. The lifetimes of the triplet states are: 83μsec, 870μsec and 8.8msec in CaF_2 and 59μsec, 640μsec and 7.7msec in SrF_2 . These metastable states have been detected by EPR and shown to have the self-trapped hole aligned along a $\langle 111 \rangle$ direction with inequivalent anion sites, resembling an H center, with a large perturbation nearby due to the F center[6]. A large Stoke's shift is observed between the absorption and emission band peaks suggesting that this phenomenon is due to exciton self-trapping as in the alkali halides[10].

Williams *et al*[10] have identified four possible, inequivalent, configurations of the F-H center pair. These are shown in Figures 2(b)–2(e) and have been labelled by him.

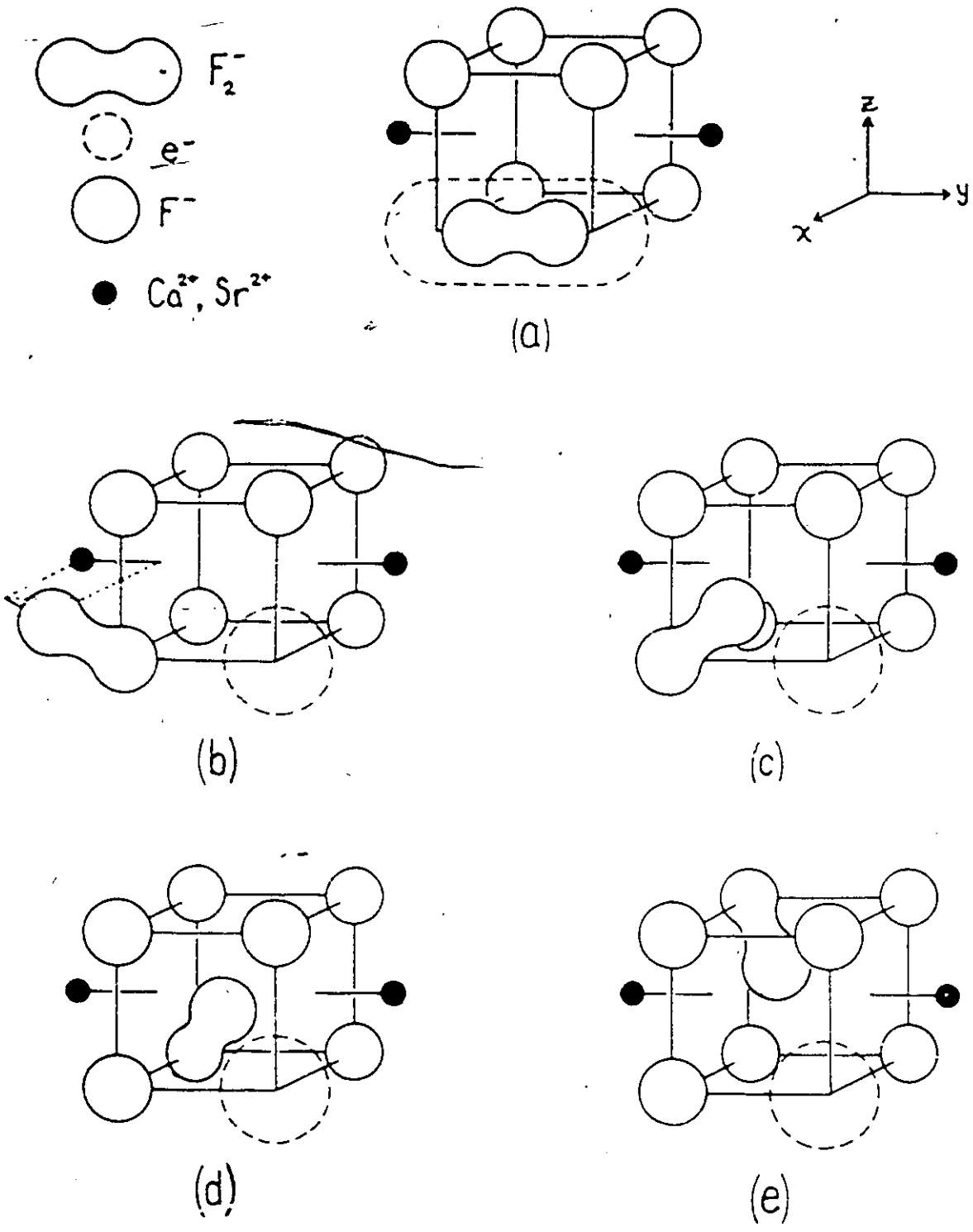

Figure 2

(V_k + e^-) and four configurations of the F-H center pair. Configurations (b)–(e) are numbered 1–4 respectively.

Configuration 4 has been included for the sake of completeness, however it is inconsistent with the EPR data because it contains a three-fold axis of symmetry. We shall not study this configuration any further.

Eshita *et al*[11,12] have associated the metastable decay components of the emission spectrum with the three inequivalent configurations. They observed that optical excitation of the F center in one configuration at low temperatures, may convert it into a different configuration. This means that in the configuration coordinate model, where the energy of a state depends on the coordinates of all ions surrounding and including the defect, there exists paths leading from the excited states in one configuration to states in different configurations.

In this work, we shall attempt to study these effects from a theoretical point of view in the hope of providing more insight into the electronic states and formation processes of the stable F-H pair. The electron wavefunction and accompanying lattice distortion will be determined self consistently. Self-consistency has shown to be important in a calculation such as this[8,13,14] because of the strong interaction of the electron with the lattice, *ie.* it is the presence of the excited electron that determines the lattice distortion in a critical way.

We shall minimize the total energy of the system by an efficient 5-point interpolation scheme that involves calculating the gradient of the energy surface in three dimensions followed by a quadratic fit in the direction of steepest descent. We simultaneously vary the positions of the lattice ions and the electron wavefunction in a consistent way.

The total energy is taken to be the sum of the lattice energy, the energy of the

defect electron and the polarization energy. The energy of the distorted lattice is made up of the electrostatic Coulomb energy, which we calculate by interpolating the Madelung potential, and the short range repulsive interaction of the ion cores, which we represent using the Born-Mayer potential. The polarization energy is calculated by a lowest-order Mott-Littleton approach and is a small contribution to the total energy. Details of these calculations will be presented in Chapter II.

The energy of the defect electron is calculated using a hybrid pseudopotential method in the extended-ion model, based on the one-electron Hartree-Fock approximation. We use the unscaled ion-size parameters of Bartram, Stoneham and Gash[23,24] to represent the interaction of the compact deep core orbitals of the lattice ions with the electron. The interaction of the more diffuse outer s and p electrons of the lattice ions is calculated quite accurately using interpolation formulae. The calculation of the electron energy is made expedient by the exclusive use of floating $1s$ gaussians to represent the electron. Using gaussians allows the integrals involved to be calculated analytically and efficiently, while floating gaussians are flexible enough to represent the electron in the low symmetry of the distorted lattice configuration.

In a preliminary work[13] using the ion-size parameters to represent both the deep core and outer s and p orbitals of the ions, we found that upon capture of an electron by the V_k center, the molecule spontaneously undergoes a combined translation and rotation finally settling along a $\langle 111 \rangle$ axis, in complete agreement with experiment. In the present work, a more detailed calculation is performed using the extended-ion model. This confirms the earlier result that the STE is effectively a nearest neighbour F center and H center

along (111), in agreement with experiment. The absorption spectrum of the F center is calculated and shown to have reasonable agreement with experiment. We also calculate the adiabatic potential curves of the ground and excited states between configurations 2 and 3 and between configurations 2 and 1. We found that these are quite flat and conversion between configurations upon optical excitation is possible. We report detailed results in Chapter III.

The present method has also been used with considerable success in treating the STE in alkali halides showing for the first time that the STE is off-centered at equilibrium resembling an F-H center pair. It demonstrated convincingly that in systems such as these, the defect electron induces large lattice distortions and that it is important to treat these in a self consistent way[8,9].

CHAPTER II - *Method of Calculation*

In order to calculate the equilibrium configuration of the defect system, we minimize the total energy as a function of the positions of the lattice ions. The total energy is the sum of up to four parts: (i) the electrostatic Coulomb energy of the ions in the lattice; (ii) the short range repulsion between ions; (iii) the energy of the defect electron and (iv) the polarization energy of the crystal. This last energy is not always included in the calculation depending on the degree of accuracy required.

We consider the interaction of the defect with a cluster of approximately 200–300 ions surrounding the defect center. The cluster size is chosen such that all significant ion interactions are included in the total energy. We take the zero of energy to be the energy of the perfect lattice, the perfect lattice being all ions at their undisplaced positions and without the V_k or F centers.

The ions immediately surrounding the defect are allowed to relax. This includes nearest neighbours and sometimes next-nearest neighbours of the F and H centers. In this way, we create a multi-dimensional space in which the energy is minimized, since each ion allowed to move contributes three degrees of freedom. The number of ions allowed to move in this set of calculations were in the 20–30 range, depending on the configuration in question.

The main feature of this method is that the lattice distortion and the electron wavefunction are treated self-consistently. Past experience with alkali halides[8] has shown that this is essential to this type of problem, since the electron wavefunction changes considerably as ions move about the lattice. Other calculations on alkali halides which determined

the lattice distortion and electron wavefunction separately[15] found that there was no axial shift of the V_k center, while the present self-consistent calculation correctly showed that the equilibrium position was off-centered due to the strong interaction of the electron with the surrounding lattice[8,9].

II.1 Lattice Coulomb Energy

The electrostatic Coulomb energy is calculated by considering an infinite lattice of point charges. We first calculate the Madelung potential of each of the ions (hence the energy when multiplied by the ion's charge) and then sum these to obtain the total Coulomb energy. Care must be taken so as not to double count interactions, since the Madelung potential is the potential produced by an infinite lattice at one ion site.

For ions that remain at their perfect lattice sites the potential is simply the Madelung constant α_M divided by the nearest-neighbour distance. For ions that have been displaced from their perfect lattice site, we expand the Madelung potential in cubic harmonics[16].

In this method, the Coulomb potential produced by a point ion lattice is expanded in a power series of the distance from a specified point, in a specified direction. The coefficients of the expansion are expressed in terms of Legendre polynomials, and involve a sum over the set of primitive lattice vectors and all unit cells. This sum is generally slow to converge, but it can be made rapidly convergent by converting it to a sum over primitive lattice vectors and reciprocal lattice vectors[17,18].

Basically, what the method reduces to is to replace the slowly converging sum:

$$V(\vec{r}) = \sum_i \frac{q_i}{|\vec{r} - \vec{R}_i|} \tag{2.1}$$

by the power series:

$$V(r) = \sum_{l=0}^{\infty} \frac{e}{d_{nn}} a_l \left(\frac{r}{d_{nn}}\right)^l \tag{2.2}$$

where d_{nn} is the nearest neighbour distance. a_l are the coefficients specific to a certain direction and are determined by the lattice structure.

In this work, we are dealing with crystals of cubic symmetry. We can then convert equation (2.2) to a sum over cubic harmonics so that this potential can be interpolated in any general direction using one set of coefficients. Thus we let:

$$V(\vec{r}) = \sum_{l=0}^{\infty} \frac{e}{d_{nn}} b_l Y_l(\vec{r}) \left(\frac{r}{d_{nn}}\right)^l . \tag{2.3}$$

The coefficients for the fluorite structure are given in Table II.1. We used terms of up to tenth order in this work. Note that b_0 is simply the Madelung constant.

Table II.1

Madelung potential interpolation coefficients for fluorite structure (atomic units). B.C.I. means body-centered interstitial site.

Coefficient	Cation Site	Anion Site	B.C.I. Site
b_0	-3.276110	1.762675	-0.249239
b_3	0.000000	21.603238	0.000000
b_4	1.399145	-2.270779	3.142413
b_6	-0.483126	0.392747	-0.302367
b_7	0.000000	-11.830096	0.000000
b_8	-0.278946	0.077396	0.124153
b_{10}	0.267278	0.000000	0.319207

It is important to note that this method may be used to find the potential produced by an infinite lattice at any point within the unit cell.

This interpolated potential is then corrected for the displacement of the other ions that have been moved, since the interpolation formula assumes all other ions are at their

perfect lattice sites. The energy is then calculated and added to the total.

II.2 Repulsive Energy

The short range repulsion of ion cores is expressed in the Born-Mayer form[19] :

$$V_{ij} = A_{ij} e^{-r/\rho_{ij}} \tag{2.4}$$

where r is the separation of ions i and j, and A_{ij} and ρ_{ij} are constants characteristic of each ion pair.

This form of the potential between closed shell ions is predicted from quantum mechanics. The values of the coefficients we used are shown in Table II.2. They were calculated by the method of Reitz, Seitz and Genberg[19] from the elastic constant, the elastic shear constant and the bulk modulus of the crystal, these being given by Hayes[1] . This method entails separating the repulsive and electrostatic contributions to the elastic constants and solving a set of three simultaneous equations for the Born-Mayer constants.

Table II.2
Repulsive constants (atomic units).

Crystal	ρ	A_{+-}	A_{--}	A_{++}
CaF_2	0.529	70.879	23.856	0.000
SrF_2	0.554	78.170	14.260	0.000

The cation-cation interaction has been excluded since the distance between positive ions is much larger than the cation-anion distance. Also, the ionic radius of the cations is smaller than that of the anions. It is estimated that A_{++}/A_{--} is of the order of 10% .

II.3 Electron Energy

To calculate the energy (and structure) of the defect electron, we use the extended ion method which is based the one electron Hartree-Fock approximation. With our hybrid pseudo-potential version of this method[8,20,21,22] , the interaction of the electron with the deep core orbitals of the lattice ions are treated with the ion-size parameters of Bartram, Stoneham and Gash[23,24] while the outer s and p orbitals are treated with interpolation formulae.

We start with the Schrödinger equation:

$$(T+V)\Psi = E\Psi \tag{2.5}$$

where V is the standard one electron Hartree-Fock potential operator given by equation 2.6:

$$V(r)|\Psi(r)\rangle = V_n(r)|\Psi(r)\rangle + \sum_{\gamma,\lambda}\Big[\langle\chi_{\gamma,\lambda}(r_1)|\frac{1}{|\vec{r}-\vec{r}_1|}|\chi_{\gamma,\lambda}(r_1)\rangle|\Psi(r)\rangle - |\chi_{\gamma,\lambda}(r)\rangle\langle\chi_{\gamma,\lambda}(r_1)|\frac{1}{|\vec{r}-\vec{r}_1|}|\Psi(r)\rangle\Big] \tag{2.6}$$

where V_n is the potential in the field of all nuclei, and $\chi_{\gamma,\lambda}$ is the λ^{th} orbital on the γ^{th} atom. The last two terms are the screened Coulomb and exchange terms.

We shall rewrite this potential in the Phillips-Kleinman pseudopotential formalism:

$$V = V_{PI} + (V - V_{PI}) \tag{2.7}$$

where V_{PI} is the point ion potential. The other term, $(V - V_{PI})$, is the short range potential, which has a much smaller contribution to V than V_{PI}. The short range potential includes the screened Coulomb and exchange interactions of the electron with the ion cores.

The N-electron formulation of the F center problem would require that Ψ include all electrons in the lattice, which is obviously prohibitive. A major simplification results by using the one electron approach for the defect electron, since the core orbitals are not expected to change very much in the presence of a defect. We thus replace Ψ by a pseudo-wavefunction ψ, already orthogonal to all the ionic orbitals:

$$|\psi\rangle = |\phi\rangle - \sum_{\gamma,\lambda} |\chi_{\gamma,\lambda}\rangle\langle\chi_{\gamma,\lambda}|\phi\rangle. \tag{2.8}$$

Up to this point, ϕ remains arbitrary. The only restriction that we shall impose upon ϕ is that it be slowly varying in the region of the core orbitals (see below). We shall use a linear combination of floating $1s$ gaussians ($e^{-\alpha r^2}$) to represent ϕ, which, along with the energy of the state ψ, is completely determined when the Schrödinger equation is solved.

The use of gaussians to represent the electron greatly simplifies the calculation, since integrals involving gaussians can be solved analytically. Another useful property of gaussians is that the product of two gaussians centered at any site, is itself a gaussian centered at a third site. Details of gaussian mathematics are outlined in Appendix A.

We use floating (or distributed) gaussian type orbitals because we may optimize ϕ by placing the gaussian centers at appropriate positions in the crystal to best represent the state of the F center in question. This gives us the required flexibility to do a self-consistent calculation, since the electron wavefunction may change considerably as the defect and lattice distortions evolve. The exclusive use of $1s$ gaussians further simplifies the calculations. Higher states can be built up from several $1s$ gaussians, however the more complex a state is the greater the number of gaussians are needed to represent it.

Therefore we define ϕ to be:

$$\phi = \sum_i b_i e^{-\alpha_i(\vec{r}-\vec{R}_i)^2} \tag{2.9}$$

where α_i are the gaussians' exponents and $\vec{R}_i$ are the gaussians' positions, both of which are parameters to be optimized. The b_i are the coefficients of the linear combination which are found when the secular determinant is solved.

The problem reduces to solving the secular equation for the state ϕ and it's energy E:

$$|H_{ij} - ES_{ij}| = 0 \tag{2.10}$$

where:

$$H_{ij} = \langle\phi_i|T|\phi_j\rangle + \langle\phi_i|V_{PI}|\phi_j\rangle + \langle\phi_i|(V - V_{PI})|\phi_j\rangle$$
$$- \sum_{\gamma,\lambda} E_{\gamma,\lambda}\langle\phi_i|\chi_{\gamma,\lambda}\rangle\langle\chi_{\gamma,\lambda}|\phi_j\rangle \tag{2.11}$$

and:

$$S_{ij} = \langle\phi_i|\phi_j\rangle - \sum_{\gamma,\lambda}\langle\phi_i|\chi_{\gamma,\lambda}\rangle\langle\chi_{\gamma,\lambda}|\phi_j\rangle. \tag{2.12}$$

The last two terms of equation (2.11) and the last term of equation (2.12) are known collectively as the ion size terms. $E_{\gamma,\lambda}$ is the energy of the λ^{th} core orbital of ion γ in the lattice. This in turn is simply the free atomic core energy, $E^0_{\gamma,\lambda}$, shifted by the potential produced by the other ions in the lattice, ΔE_γ, which is calculated as described in Section II.1:

$$E_{\gamma,\lambda} = E^0_{\gamma,\lambda} + \Delta E_\gamma. \tag{2.13}$$

Calculation of the kinetic energy, point ion and gaussian overlap are straightforward. The derivation of these expressions is given in Appendix B.

II.3.1 Ion size terms

The ion-size terms contain sums of the contributions from core orbitals of the ions in the lattice. We rewrite these terms in the following way:

$$\sum_{\gamma,\lambda}\langle\phi_i|\chi_{\gamma,\lambda}\rangle\langle\chi_{\gamma,\lambda}|\phi_j\rangle = \sum_{\gamma} T_{\gamma}^{(1)} \tag{2.14}$$

$$\langle\phi_i|(V-V_{PI})|\phi_j\rangle - \sum_{\gamma,\lambda} E_{\gamma,\lambda}\langle\phi_i|\chi_{\gamma,\lambda}\rangle\langle\chi_{\gamma,\lambda}|\phi_j\rangle = \sum_{\gamma} T_{\gamma}^{(2)} - \sum_{\gamma}\Delta E_{\gamma} T_{\gamma}^{(1)}. \tag{2.15}$$

Here we can see that:

$$T_{\gamma}^{(1)} = \sum_{\lambda}\langle\phi_i|\chi_{\gamma,\lambda}\rangle\langle\chi_{\gamma,\lambda}|\phi_j\rangle \tag{2.16}$$

$$T_{\gamma}^{(2)} = \langle\phi_i|(V-V_{PI})_{\gamma}|\phi_j\rangle - \sum_{\lambda} E^{0}_{\gamma,\lambda}\langle\phi_i|\chi_{\gamma,\lambda}\rangle\langle\chi_{\gamma,\lambda}|\phi_j\rangle \tag{2.17}$$

contain contributions from the orbitals of only one ion at a time. We now make the approximation that ϕ_i be slowly varying in the region of the core orbitals to expand ϕ_i as a mutilpolar series, followed by a Taylor series expansion about R_i. Since ϕ_i is slowly varying, ϕ_i and it's first derivative can be taken to be constants. The integrations over the core orbitals is then performed to come up with the so-called ion-size parameters. Note that these parameters are properties of each individual ion and has no dependence on the pseudo-wavefunction used, provided that this is slowly-varying.

Equations (2.16) and (2.17) may then be rewritten in the much simpler form:

$$T_{\gamma}^{(1)} = f_1 B_{\gamma} + f_2 K'_{\gamma} + f_3 K_{\gamma} + \cdots \tag{2.18}$$

$$T_{\gamma}^{(2)} = f_1 A_{\gamma} + f_2 J'_{\gamma} + f_3 J_{\gamma} + \cdots \tag{2.19}$$

The A, B, J, K, J', K' are the ion-size parameters. A, J, J' represent the short range potential $(V - V_{PI})$ while B, K, K' represent the overlaps of the gaussians with the core

orbitals. The f_1, f_2 and f_3 are functions depending solely on the gaussians (and it's derivatives) and the vector joining them to the ion site. Details of the derivation of these parameters can be found in Appendix B and in the references[20,21,23,24].

It was discovered that when all core orbitals were included in the ion-size parameters, the convergence of higher order terms was questionable, *ie.* K, K', J, J' were as large or larger than A and B. When the outer s and p (OSP) electrons were excluded from the sums of equations (2.16) and (2.17), convergence was much more rapid. This is due to the diffuse nature of the OSP electrons as opposed to the more compact deep core electrons. With diffuse OSP electrons, the slowly varying approximation breaks down[14,20,21].

This was the motivation to develop the hybrid pseudopotential scheme. In this method, we use the first two orders of the ion-size parameters for the deep core electrons (by restricting the sums of equations (2.16) and (2.17) to deep cores only), while the OSP shells are calculated explicitly by interpolation. The interpolation formulae will be described below. The ion-size parameters we used in this calculation can be found in Table II.3.

Table II.3

Deep core ion-size parameters for fluorite structure (atomic units).

Ion	A	B	J	K	J'	K'
Ca^{2+}	26.77859	1.70488	1.93452	0.16146	3.63728	0.23421
Sr^{2+}	40.78775	3.47726	6.53412	0.75885	3.38879	0.36240
F^-	7.95117	0.34943	-0.00794	0.00000	0.54139	0.02252

For all the above core wavefunctions (Ca^{2+}, Sr^{2+}, F^-) we used atomic orbitals obtained from a self-consistent field (SCF) calculation. A computer code from Muhlhausen

and Gordon which takes into account the point-ion potential of the lattice was used for this purpose[25] . An anion, surrounded by cations in the lattice, is sitting at a potential well which has the effect of compacting the wavefunction slightly. Cations, on the other hand are at a potential barrier which expands the wavefunction. This effect is more pronounced for anions than cations. For Sr^{2+} we used the atomic SCF orbitals of Clementi and Roetti[26] . For Ca^{2+} and F^- we initially used orbitals from Harker[27] , however it was found that these wavefunctions were too diffuse for ions in a lattice. Therefore the orbitals were recalculated using the SCF program in the presence of a square potential well (or barrier). The resulting wavefunctions are used in equations (2.16) and (2.17) but note that the energy to be used in equation (2.17) is the free atomic core energy.

II.3.2 Interpolation Formulae

The interpolation of $(V - V_{PI})$ and $\langle\phi|\chi_{\gamma,\lambda}\rangle$ was treated in the following way. We separate the screened Coulomb and exchange parts of the short range potential. The screened Coulomb term, in it's exact form, is an expression such as:

$$\langle\phi_i|V_{sc,\gamma}|\phi_j\rangle = \sum_{\lambda}^{OSP} \int \frac{\langle\phi_i|\chi_{\gamma,\lambda}\rangle\langle\chi_{\gamma,\lambda}|\phi_j\rangle}{r}\, d\tau \tag{2.20}$$

and this was fitted to an interpolation formula:

$$\langle\phi_i|V_{sc\gamma}|\phi_j\rangle = \int \phi_i^* \frac{A_{sc,\gamma} e^{-\beta_{sc,\gamma}(\vec{r}-\vec{R}_\gamma)^2}}{r} \phi_j\, d\tau. \tag{2.21}$$

The parameters of the interpolation, $A_{sc,\gamma}$ and $\beta_{sc,\gamma}$ for any ion γ were determined in the following way: first, the outer s and p orbitals (in their Slater form as given by the SCF calculation) were fitted to a large number of gaussians (10–20). This amounts to changing the basis of the orbitals. The exact value of the screened Coulomb interaction

due to both OSP orbitals was calculated for a range of the gaussians' α_i and R_i of ϕ_i, so that the interpolation formula will be applicable to all ions of the same type as ion γ. We then perform a least squares fit to determine the constants $A_{ec,\gamma}$ and $\beta_{ec,\gamma}$. Since $\phi_i\phi_j = k\phi_k$, we have only to fit $\int \phi_k A e^{-\alpha r^2}/r\, d\tau$ rather than the more complicated formula $\int \phi_i A e^{-\alpha r^2}/r\phi_j\, d\tau$; this is one example of the usefulness of gaussians. Using this procedure, we obtained quite satisfactory fits, with RMS deviations better than 10^{-3} in all cases. The values of the fitted parameters can be found in Table II.4.

The exchange interaction was interpolated in much the same way. The exact form of the exchange potential is:

$$\langle\phi_i|V_{ex,\gamma}|\phi_j\rangle = \sum_{\lambda}^{OSP} \int \frac{\langle\phi_i(r_2)|\chi_{\gamma,\lambda}(r_1)\rangle\langle\chi_{\gamma,\lambda}(r_2)|\phi_j(r_1)\rangle}{|\vec{r}_1 - \vec{r}_2|}\, d\tau_1\, d\tau_2 \qquad (2.22)$$

and we fit this to an expression of the form:

$$\langle\phi_i|V_{ex,\gamma}|\phi_j\rangle = \int \phi_i^* A_{ex,\gamma} e^{-\beta_{ex,\gamma}(\vec{r}-\vec{R}_\gamma)^2}\phi_j\, d\tau. \qquad (2.23)$$

Here the gaussian product rule does not apply to the exact form of the exchange (equation (2.22)) since this is a two electron integral and the integration is over different coordinates. However it was found that the quality of the fit for the off-diagonal elements was comparable to the accuracy of the diagonal elements so that again we had only to fit $\int \phi_i V_{ex}\, d\tau$. The RMS deviation in all cases was better than 10^{-2}. The values of A_{ex} and β_{ex} are listed in Table II.4.

The overlap integrals are terms of the form

$$ss\sigma = \int \phi_i^* \chi_s(r)\, d\tau \qquad \text{and} \qquad sp\sigma = \int \phi_i^* \chi_p(r)\, d\tau. \qquad (2.24)$$

Table II.4

Short range potential interpolation parameters for fluorite structure (atomic units).

Ion	β_{sc}	A_{sc}	β_{cx}	A_{cx}
Ca^{2+}	1.14560	-5.49402	0.44400	-2.37786
Sr^{2+}	1.11840	-5.62715	0.38480	-2.18423
F^-	0.76000	-3.82315	0.37520	-2.07188

Here we fit the overlap of a single gaussian with the outer s and p states separately. Only the $sp\sigma$ integral need be calculated because the $sp\pi$ integral is 0 by symmetry. Any general sp overlap may be decomposed into it's σ and π components and only the $sp\sigma$ will be non-zero.

It was found that an interpolation formula using one gaussian to represent the core states was inadequate compared to the accuracy of the screened Coulomb and exchange terms. However, two gaussians with their exponents related by a simple ratio gave fits of sufficient accuracy. Therefore we used the simple form of equation (2.25) to represent the overlap with the outer s core states:

$$ss\sigma \Rightarrow \langle\phi_i|\chi_s\rangle = N\int \phi_i^* \left[N_1 e^{-\beta_{soul}r^2} + A_{soul}N_2 e^{-\beta_{soul}r^2/\rho_s}\right] d\tau. \qquad (2.25)$$

Here ρ_s is the ratio of the exponents of the two fitted gaussians, which is a parameter that is adjusted to give the best least squares fit. Usually $\rho = 4$ gave the best fit, however in one case $\rho = 8$ gave the best fit. A_{soul} and β_{soul} are parameters determined by the least squares fitting procedure. N_1, N_2 and N are normalization factors determined by the other parameters of the equation.

Similarly, the overlap with the outer p shell is fitted to a function of the form:

$$sp\pi \Rightarrow \langle\phi_i|\chi_{pz}\rangle = N'\int \phi_i^* \left[N_1' e^{-\beta_{poul}r^2} + A_{poul}N_2' e^{-\beta_{poul}r^2/\rho_p}\right] \cdot z\, d\tau. \qquad (2.26)$$

Here all the paramters are determined in the same way as for the s shell overlap.

The accuracy of the s overlap was better than 10^{-3} RMS deviation in all cases, while for the p shell overlap the fit was slightly better with the RMS deviation generally being one order of magnitude lower. The values of the overlap parameters are given in Table II.5.

Table II.5

Overlap interpolation parameters for fluorite structure (atomic units).

Ion	β_{sovl}	β_{povl}	ρ_s	ρ_p	A_{sovl}	A_{povl}	E_s	E_p
Ca^{2+}	0.65	0.65	4	4	0.12142	0.08017	-2.82800	-1.93000
Sr^{2+}	0.85	0.70	4	4	0.67491	0.09251	-2.37561	-1.57866
F^-	0.85	1.20	4	8	0.38138	0.44265	-1.06574	-0.17442

In earlier works, the β was taken to be the same for both the s and p orbitals and $\rho = 4$ was used in all cases. However, we found that the increase in the accuracy of the fit by increasing the number of adjustable parameters from 3 to 6 was justified. E_s and E_p are the energies of the OSP orbitals which are required in the evaluation of equation (2.13).

II.3.3 Treatment of the V_k center

The V_k center demands special attention with our hybrid method since it consists of two ions bound together. Yet, we wish to keep the treatment of the molecule as close as possible to the treatment of the individual ions to simplify the calculation. We shall treat the V_k center as a pair of $F^{-\frac{1}{2}}$ ions with their own set of parameters.

In this case, molecular orbitals were used as opposed to the atomic orbitals of individual ions. These have been calculated by Gilbert and Wahl[28] . The molecular orbitals are composed of a linear combination of atomic orbitals centered on two sites.

By decomposing the molecular orbitals into their constituent atomic orbitals, we can

calculate the ion-size parameters in much the same way as for individual ions. However, the same problem with the slowly-varying approximation and the diffuse character of the outer orbitals is encountered. Since it is the outer σ and π orbitals that take part in the binding of the molecule, and we expect the deep cores of the ions making up the molecule to remain largely unchanged, we used the deep core ion-size parameters of F^- for the ions of F_2^-, and we again use interpolation formulae for the OSP orbitals.

With the molecule, there are eight OSP molecular orbitals Ψ, namely:

(1) $$\Psi(\sigma_g 2s) = \frac{[\chi_s(r_A) + \chi_s(r_B)]}{\sqrt{2(1+O_s)}}$$

which is the even combination of atomic $2s$ orbitals centered on ions at $\vec{R}_A$ and $\vec{R}_B$. We define $\vec{r}_A = \vec{r} - \vec{R}_A$. O_s will be defined below. The odd combination is used as well:

(2) $$\Psi(\sigma_u 2s) = \frac{[\chi_s(r_A) - \chi_s(r_B)]}{\sqrt{2(1-O_s)}}$$

There are six combinations of orbitals involving the three different p states centered on the two sites:

(3) $$\Psi(\sigma_u 2p_z) = \frac{[\chi_{p_z}(r_A) + \chi_{p_z}(r_B)]}{\sqrt{2(1+O_{p_z})}}$$

(4) $$\Psi(\sigma_g 2p_z) = \frac{[\chi_{p_z}(r_A) - \chi_{p_z}(r_B)]}{\sqrt{2(1-O_{p_z})}}$$

where we have defined the z-axis to be the axis of the molecule.

(5,6) $$\Psi(\pi_u 2p_\mu) = \frac{[\chi_{p_\mu}(r_A) + \chi_{p_\mu}(r_B)]}{\sqrt{2(1+O_{p_\mu})}}$$

(7,8) $$\Psi(\pi_g 2p_\mu) = \frac{[\chi_{p_\mu}(r_A) - \chi_{p_\mu}(r_B)]}{\sqrt{2(1-O_{p_\mu})}}$$

where μ is either x or y.

Here we have defined:

$$O_\lambda = \langle \chi_\lambda(r_A) | \chi_\lambda(r_B) \rangle \tag{2.27}$$

and $1/\sqrt{2(1 \pm O_\lambda)}$ is the normalization factor for the molecular orbitals. We assume that the three p type orbitals are degenerate.

In an earlier work[8] , the overlap integrals with the molecular orbitals were calculated exactly (no interpolation). This complicated the calculation somewhat with very little change in the results, so we decided to continue with the hybrid scheme for the V_k center.

At this point, we will make the assumption that $O_\lambda = 0$ for all λ to simplify the calculation. We investigated the effect of this approximation by calculating the value of O_λ explicitly, then calculating the exact value of an overlap of the molecular p orbitals with a $1s$ gaussian, $\langle \phi_i | \Psi_p^{MO} \rangle$, and comparing this result with our approximated result. The gaussian was placed along the axis of the molecule at a distance of half the separation of the two ions of the molecule. For the worst case, with O_{p_x}, we found that our approximation underestimated the exact overlap by 14%. For the other p states, O_{p_z} and O_{p_y}, we found that the approximation overestimated the correct value by about 5%. When the effects of all three p states are combined, as will be the case in our interpolation formula for the V_k center, the net error was reduced to about 2%. That is, the errors due to our approximation systematically cancel each other out. This fact, in combination with the small contribution of the ion-size terms to the total energy, justifies the approximation.

In the same manner as for individual ions, the OSP atomic orbitals of each ion of the molecule are fitted to 10–20 gaussians. We could then fit the screened Coulomb and

exchange terms as before, however we obtained a better fit if we used an extra term in the interpolation formula at the center of mass of the molecule. This extra term accounts for the cross term when these potentials are calculated using molecular orbitals. Details of the derivation of these terms are given in Appendix C.

Therefore, for the screened Coulomb interaction we use an interpolation formula of the form:

$$V_{sc}^{MO} = \frac{A_{sc}e^{-\beta_{sc}|\vec{r}-\vec{R}_A|^2}}{|\vec{r}-\vec{R}_A|} + \frac{A_{sc}e^{-\beta_{sc}|\vec{r}-\vec{R}_B|^2}}{|\vec{r}-\vec{R}_B|} + \frac{A'_{sc}e^{-\beta'_{sc}|\vec{r}-\vec{R}_{com}|^2}}{|\vec{r}-\vec{R}_{com}|} \qquad (2.28)$$

while for the exchange interaction the interpolation formula is:

$$V_{ex}^{MO} = A_{ex}e^{-\beta_{ex}|\vec{r}-\vec{R}_A|^2} + A_{ex}e^{-\beta_{ex}|\vec{r}-\vec{R}_B|^2} + A'_{ex}e^{-\beta'_{ex}|\vec{r}-\vec{R}_{com}|^2}. \qquad (2.29)$$

Here, $\vec{R}_{com} = (\vec{R}_A + \vec{R}_B)/2$ is the center of mass position of the molecule. The constants A_{sc}, A'_{sc}, A_{ex}, A'_{ex} and the β's are determined in the same way as for individual ions using a least squares approach, except that in this case the number of parameters to be fitted has doubled. The values that we found gave the best fit are shown in Table II.6. The RMS deviation for these terms was better than 10^{-3} for both the exchange and screened Coulomb terms.

Table II.6

F_2^- short range potential interpolation coefficients (atomic units).

Int. Site	β_{sc}	A_{sc}	β_{ex}	A_{ex}
Ion site	1.10000	-4.13804	0.42667	-2.30630
C.O.M. site	0.13333	-0.14872	0.83333	0.33918

The overlap of the gaussians with the molecular OSP orbitals becomes a simple ex-

pression in light of our overlap approximation described above:

$$\begin{aligned}\langle\phi_i|\Psi_\lambda^{MO}\rangle &= \frac{\langle\phi_i|\chi_\lambda(r_A) \pm \chi_\lambda(r_B)\rangle}{\sqrt{2(1 \pm O_\lambda)}} \\ &\approx \frac{1}{\sqrt{2}}\langle\phi_i|\chi_\lambda(r_A)\rangle \pm \frac{1}{\sqrt{2}}\langle\phi_i|\chi_\lambda(r_B)\rangle\end{aligned} \tag{2.30}$$

which can be fitted to exactly the same interpolation formula that was used for the individual ions (equations (2.25) and (2.26)). The factor of $(1/\sqrt{2})$ is cancelled when the full expression for the overlap term is calculated in equations (2.11) and (2.12): $\sum_\lambda \langle\phi_i|\Psi_\lambda\rangle\langle\Psi_\lambda|\phi_j\rangle$ makes it a factor of 1/2, which is cancelled when the g and u orbitals are counted. The values of the overlap interpolation coefficients are given in Table II.7. For this fit the RMS deviation was better than 10^{-3}.

Table II.7

Overlap interpolation parameters for V_k center, F_2^- (atomic units).

β_{sovl}	β_{povl}	ρ_s	ρ_p	A_{sovl}	A_{povl}	E_s	E_p
0.70	0.70	4	4	0.15134	0.25279	-1.19526	-0.30194

Throughout all of the above discussion, we have assumed that the V_k center is perfectly symmetrical, *ie.* the hole charge is shared equally between both ions of the molecule. However, in most cases this isn't true, as the charge is shifted more to one side than the other, changing the molecular orbitals. At present we have no means of treating this problem in the extended ion method. One possible way to deal with this would be to scale all of the parameters in some way from an F^- ion to $F^{-\frac{1}{2}}$ to F^0 as the charges shift from one side to the other. However this is beyond the scope of this work.

The charge distribution in the H center, Z, which we use in our calculations has been calculated by Parker *et al*[4] . We define Z such that the charge on the interstitial ion

is $-(1-Z)$ and the charge on the substitutional ion is $-Z$. For SrF_2 , $Z = 0.69$ while for CaF_2 $Z = 0.76$. This means that the interstitial ion has a net charge of -0.31 in SrF_2 (-0.24 for CaF_2) while the other ion has a charge of -0.69 (-0.76). The charge distribution is determined mainly form the potential difference at the two sites.

II.4 Polarisation Energy

We calculate the polarisation energy by the Mott-Littleton method of the lowest order[29] . We assume that the ions behave as point dipoles with polarisability equal to the free atomic polarisability .

The polarisation energy is given by:

$$E_{pol} = -\frac{1}{2}\sum_{\gamma} \vec{E}_{loc}(\vec{R}_\gamma)\cdot\vec{\mu}(\vec{R}_\gamma) + \text{ dipole} - \text{dipole terms.} \tag{2.31}$$

We shall neglect the higher order dipole-dipole interaction. $\vec{E}_{loc}$ is the local electric field produced by all other ions and the F center in the neighborhood of an ion at $\vec{R}_\gamma$. $\vec{\mu}(\vec{R}_\gamma)$ is the dipole moment induced on the ion at $\vec{R}_\gamma$ and is given by:

$$\vec{\mu}(\vec{R}_\gamma) = \alpha_\gamma \vec{E}_{loc}(\vec{R}_\gamma) \tag{2.32}$$

where α_γ is the free atomic polarisability of ion γ. Therefore, we may rewrite the polarisation energy as:

$$E_{pol} = -\frac{1}{2}\sum_{\gamma} \alpha_\gamma \vec{E}^2_{loc}(\vec{R}_\gamma) \tag{2.33}$$

There are two main contributions to the local electric field at any ion site: (1) the electric field due to lattice distortions and (2) the electric field produced by the defect electron.

First, consider the electric field at a perfect lattice site in a perfect lattice (no distortion, no defect). In this case there would be no electric field at this sampling point since the field produced by any one ion in the lattice is exactly cancelled by other ions in the lattice. Now if an ion of charge q is displaced from it's perfect lattice site, the sampling ion will "see" the real charge q at it's new position, as well as an image charge $-q$ at the original position due to the surrounding lattice. Both of these "charges" will then contribute to the local electric field at the sampling point. We use this method to calculate the electric field at ions outside of the small cluster of nearest-neighbour ions that have been allowed to relax.

Now consider sampling the electric field away from a perfect lattice site, as is the case for the ions allowed to move. At these points the simple method described above does not apply because of the lower symmetry of the new sampling position. In this case we use the fact that:

$$\vec{E}_{loc} = -\nabla V_{loc} \tag{2.34}$$

where V_{loc} is the potential at the sampling point. We calculate the gradient of V_{loc} in the immediate neighbourhood of the ion in question by a linear interpolation in three dimensions:

$$V_{loc} = a + bx + cy + dz. \tag{2.35}$$

This requires the potential to be calculated at four points to solve for the four unknown coefficients a, b, c and d. The calculation of the potential is done by the same method as described in section II.1.

By the definition of the derivative, the potential's sampling points should be close

together. We are limited in this respect by the loss in accuracy of the resulting coefficients due to round-off errors. Once the coefficients have been calculated it is easy to calculate the electric field.

The contribution to the electric field due to the defect electron is straightforward. We use the electron wavefunction that is obtained from the electron energy calculation. In this approximation, we will neglect the core orthogonalization of the wavefunction, as this would complicate matters too much. Therefore we first renormalize the electron wavefunction. Then we use Gauss' law to determine the electric field produced by the electron.

The charge density is given by

$$\begin{aligned} \rho(\vec{r}) &= \psi^2(\vec{r}) \\ &= \left| \sum_i c_i e^{-\alpha_i(\vec{r}-\vec{R}_i)^2} \right|^2 \\ &= \sum_k d_k e^{-\alpha_k(\vec{r}-\vec{R}_k)^2} \end{aligned} \tag{2.36}$$

by the gaussian product rule. The charge enclosed in a sphere of radius $|\vec{r}_k - \vec{R}_\gamma|$ due to the gaussian k is:

$$Q_k(\vec{R}_\gamma) = \int^{\vec{R}_\gamma} e^{-\alpha_k(\vec{r}'-\vec{R}_k)^2}\, d\tau' \tag{2.37}$$

and the electric field will be given by:

$$\vec{E}_{loc}(\vec{R}_\gamma) = -\sum_k d_k \frac{Q_k(\vec{R}_\gamma)}{|\vec{R}_\gamma - \vec{R}_k|^3}(\vec{R}_\gamma - \vec{R}_k) \tag{2.38}$$

The field produced by the defect electron is added to the field produced by the lattice distortion and the polarisation energy is then summed over all ions. We limit this sum

in practice to the large cluster of 200–300 ions. The neglect of the outer ions is justified because the defect system is electrically neutral.

The free atomic polarisabilities that we used in this work are shown in Table II.8. They are taken from Tessman *et al*[43] .

Table II.8
Free atomic polarisabilities for fluorite structure (atomic units)[3].

Ion	α
Ca^{2+}	7.42
Sr^{2+}	10.80
F^-	4.40

II.5 Minimization method

Now that we know how to calculate the energy, there remains the question of finding the minimum energy configuration of the multidimensional space of the crystal. To solve this problem we developped the following minimization procedure. We always minimize with respect to the total energy:

$$E_{total} = E_{Coul} + E_{rep} + E_{elec} + E_{pol} \tag{2.39}$$

where the various constituent energies have been described in the previous four sections.

First, we treat at most only three degrees of freedom at one time by minimizing each ion individually. The same process is carried out in sequence over all ions allowed to move. We then repeat the whole procedure and iterate until we reach convergence to within some value of the energy. Convergence was usually obtained within 3 or 4 iterations.

For this work, the V_k center has to be treated differently. It has two ions covalently bonded, each ion contributing three degrees of freedom for a total of six dimensions. This is reduced to five dimensions since we consider the two ions of the molecule to have a fixed separation. Therefore, to find the minimum energy position of the molecule, we minimize separately the center of mass position of the molecule ($\vec{R}_{com}$) and the polar angles specifying the orientation of the molecule (θ, ϕ).

We take the separation of the two ions of the molecule from the molecular orbital calculations of Gilbert and Wahl[28] which in the case of F_2^- is 3.75 (a.u.).

In general, the V_k center is displaced by large distances and it usually requires more iterations to reach equilibrium and convergence. Therefore we minimize twice over the molecule position before the rest of the lattice is minimized.

To calculate the minimum energy position, we use the following efficient interpolation scheme. The method is described here for three dimensions, but it is easily modified to any number of degrees of freedom (*eg.* 2-D for the orientation of the V_k center).

First, we interpolate the energy surface to first order the three dimensions:

$$E = a_0 + a_1 x + a_2 y + a_3 z. \tag{2.40}$$

This requires the energy to be sampled at four points. In practice we need only calculate the energy at three points since one point can be the energy before the ion is moved, which is obtained from the minimization of the previous ion. For the other three sampling points we chose three mutually perpendicular directions to avoid problems with linear independence when we solve the set of 4 simultaneous equations for the coefficients of equation (2.40). We can now calculate the direction and magnitude of the gradient of the

energy surface, ∇E, in these three dimensions. As with the polarisation energy, we must choose sampling points which are close together by the definition of the derivative, and yet not so close as to lose accuracy in the coefficients of the interpolation.

Then to calculate the minimum energy position of the ion, we interpolate to second order along a line in the direction $-\nabla E$:

$$E = a + b\delta + c\delta^2 \tag{2.41}$$

where δ is the displacement of the ion in this direction.

Here we need to evaluate the energy at only one more point since we already know a and b (a is the energy at $\delta = 0$ while $b = |\nabla E|$ at $\delta = 0$). Then it is straightforward to determine the position of minimum energy, δ_m:

$$\frac{dE}{d\delta} = 0 \quad \text{at} \quad \delta_m \quad \Longrightarrow \quad \delta_m = -\frac{b}{2c} \tag{2.42}$$

The ion is then moved a distance δ_m in the $-\nabla E$ direction. We reevaluate the energy with the ion at this position and compare it with the other energies that have been calculated in the course of the minimization, and the ion is placed at the position that gives the lowest energy.

We can determine how good (or bad) the interpolation is by evaluating equation (2.41) with $\delta = \delta_m$. In almost all cases the interpolated value is within less than 0.1% of the exact value of the energy with the ion at δ_m. Only when large displacements are involved did this rise to the order of 1%.

We shall also want to evaluate the adiabatic potential barriers along various paths through the energy surface. To do this we must restrict some coordinates to follow a

prescribed path. We will usually use the position of the V_k center for this purpose. We simply determine the path that the molecule is to move on, place it at various points along the path and allow the rest of the lattice to minimize. This describes the surface of the energy in these coordinates.

The choice of the path to use remains arbitrary. However, we usually try to find the most likely way for the molecule to get from one configuration to another.

CHAPTER III - *Results*

III.1 Defect Formation

We shall start the discussion of the results with the initial formation of the STE, *ie.* the V_k center along (100) and the electron symmetrically distributed about the V_k center as shown in Figure 2(a). We found the total energy of this state, in a perfect lattice with no distortion, to be 20.05 eV in CaF_2 and 14.49 eV in SrF_2 . The electron energy is 7.44 eV and 2.96 eV respectively.

The bases used to represent the electron in this case were two sets of 5 1*s* gaussians centered around the two perfect lattice anion sites of the V_k center. The 5 bases were placed in a tetrahedral arrangement as follows: 4 tetrahedrally arranged gaussians around a single gaussian at the anion vacancy. All 5 bases had gaussian exponents of $\alpha = 0.08$ (a.u.)$^{-2}$ and the tetrahedral bases were placed at a distance of 0.17 (a.u.) from the central one, along the (111) axes pointing towards the nearest neighbour cations. We use this arrangement of bases because it has the required symmetry of the 1*s* ground state and the electron would be expected to be attracted to the cations.

The choice of bases to use here was made by trial and error. Addition of more bases does not give a significant lowering of the electron energy. As long as the symmetry is not lowered, the electron energy remains high. When the lattice is allowed to seek a new equilibrium configuration, the electron shows a strong tendency to localize on one anion site.

The high electron energy in this symmetrical state is an indication of it's instability. The fact that the electron energy is positive shows that this configuration is not binding

for the electron. This configuration is probably not realized in the actual defect formation process, but it is a convenient starting and reference point for our calculations.

Therefore, to begin the minimization process, we started with the V_k center along $\langle 100 \rangle$, with the two sets of tetrahedral bases on both sides of the molecule and no distortion of the surrounding ions. We found that, at first, the molecule was slow to move away from its centered position, yet there was a definite preference for a lower energy position that was off-centered. As the molecule moved further away, the electron quickly began to be localized more on one side than the other. The localized electron interacts strongly with the molecule, pushing it away and forming an F center. Finally, the electron then moves almost completely to one side. Therefore, we used the set of 5 tetrahedral bases on the emerging vacancy for all further calculations to save on the computation time. This does not effect the results since we found that the same instability was present with both balanced and unbalanced bases.

The complete minimization shows that the molecule spontaneously undergoes a combined rotation and translation, and after several iterations it ends up along a $\langle 111 \rangle$ axis. Two examples of the minimization sequence are shown in Tables III.1 and III.2. Both cases involve SrF_2 with the set of 5 tetrahedral bases, on one side only, used to represent the electron.

In the first example, the molecule ends up in configuration 2. Similar results are obtained with both $Z = 0.50$ and $Z = 0.69$. To be aligned exactly along the $\langle 111 \rangle$ axis of configuration 2, $[\bar{1}11]$, with one ion at the substitutional anion site would require that $\theta = 54.74°$, $\phi = 135°$ and $\vec{R}_{com} = (-1.08, 1.08, 1.08)$(a.u.). We can see that using the equi-

Table III.1

Full minimization from the perfect lattice of SrF_2 .
System goes to configuration 2.
Energies are in eV, angles in degrees and positions in (a.u.). Details in the text.

Iteration	$\vec{R}_{com}$	θ, ϕ	E_{tot}	E_{elec}°	Z
no min. 0	(0.00, 2.90, 0.00)	90.0, 90.0	11.74	0.98	0.50
$\frac{1}{2}^{*}$	(0.00, 2.40, 0.00)	89.0, 91.0	10.74	-0.25	0.50
1	(-0.02, 1.90, 0.01)	88.0, 92.0	8.57	-1.97	0.50
2	(-0.61, 1.08, 0.10)	76.1, 96.0	8.01	-3.12	0.50
5	(-0.92, 0.83, 0.79)	55.0, 130.0	7.46	-4.63	0.50
after 6 iterations with $Z = 0.69$					
6	(-1.12, 1.09, 1.06)	54.8, 131.9	7.97	-6.64	0.69

* *Minimized over molecule coordinates once, no lattice distortion.*

librium hole charge distribution, $Z = 0.69$, gives a result with the H center closer to being exactly along the $[\bar{1}11]$ axis. (This last result, with $Z = 0.69$, was obtained using Harker's core wavefunctions before the problems with these were noticed (see section II.3.1); all other results use the recalculated SCF wavefunctions.)

We can see that the drop in total energy in going from on-centered STE to the equilibrium position in configuration 2 is due almost entirely to the drop in the electron energy. Thus the driving force of the instability is the tendency of the electron to form a stable F center. To do this, an anion vacancy must be formed, and this is accomplished by the off-centered position of the V_k center.

The second example shows the molecule ending up at the midpoint between configurations 1 and 2. This position is similar to the midpoint in the adiabatic potential curve (see section III.4 below) where the molecule may move to either configuration 1 or 2. This result was obtained using a different set of sampling points for the interpolation of the energy, *ie.* sampling on different parts of the energy surface, and using $Z = 0.50$

Table III.2

Full minimization from the perfect lattice of SrF_2 .
System goes to configuration 1.
Energies are in eV, angles in degrees and positions in (a.u.). Details in the text.

Iteration	$\vec{R}_{com}$	θ, ϕ	E_{tot}	E_{elec}	Z
no min. 0	(0.00, 2.90, 0.00)	90.0, 90.0	11.74	0.98	0.50
$\frac{1}{2}$*	(0.00, 2.40, 0.00)	89.0, 90.0	10.75	-0.25	0.50
1	(0.01, 1.40, 0.04)	90.1, 91.6	8.32	-2.50	0.50
2	(0.08, 0.76, 0.23)	92.8, 101.2	8.04	-3.13	0.50
5	(-0.06, 0.05, 1.01)	86.4, 133.8	7.57	-4.84	0.50
starting from after 2 iterations above, changing Z to 0.69					
2	(0.08, 0.76, 0.23)	92.8, 101.2	7.84	-2.55	0.69
4	(0.43, -0.46, 0.94)	112.4, 135.0	7.07	-4.80	0.69
6	(0.97, -1.08, 1.08)	124.8, 137.1	6.90	-5.28	0.69

* *Minimized over molecule coordinates once, no lattice distortion.*

throughout the minimization. If we then redistribute the hole charge distribution to the equilibrium distribution of configuration 1, the molecule then ends up in this configuration, as shown in the second half of Table III.2. Exact alignment of the H center on the $\langle 111 \rangle$ axis of configuration 1, $[1\bar{1}1]$, would require that $\theta = 125.26°$, $\phi = 135°$ and $\vec{R}_{com} = (1.08, -1.08, 1.08)$(a.u.). The variation of the energy as the molecule moves to an equilibrium is similar to the first example in that the drop in the total energy is due almost entirely to the drop in the electron energy.

This means that at some point on the energy surface the path to an equilibrium branches into two separate paths. Also, it is not unlikely that it could branch into a third path leading to configuration 3. However, this would require the molecule bond to be switched to a different pair of anions. In the present work bond switching cannot be treated, so that we have not been able to search for this third path. However, we must conclude that any one of the three configurations could be reached upon the initial

formation of the defect.

The approximations dealing with the hole charge distribution are necessary because we have no means at present of determining Z self-consistently. However the results are not strictly dependent on the hole distribution since we obtain the same results in general with both $Z = 0.50$ and $Z = 0.69$.

III.2 Ground state minimization

At equilibrium, the defect system resembles an F center and an H center in any one of the three configurations, in complete agreement with experiment[6,10]. Therefore, we then performed a more detailed minimization in each of the three configurations separately. We used the same set of 5 tetrahedral bases for all three cases. The choice of bases is again made by trial and error; it was this combination of bases which gave the lowest electron energy and it contains the proper symmetry of the ground state (see below for basis optimization). The results are not critically dependent on the placement of the basis in the ground state since other combinations of bases were tested with similar results, showing that the ground state energy is stable and easily represented.

We have used the hole distribution, Z, of the H center as calculated by Parker *et al*[4] throughout the minimization where $Z = 0.76$ in CaF_2 and $Z = 0.69$ in SrF_2 .

All three configurations started with no distortion of the lattice ions but with the V_k center aligned along the appropriate $\langle 111 \rangle$ axis. We allowed all 20–30 ions including the V_k center ions to seek out their respective minimum energy positions. The minimization sequence was iterated until we obtained convergence to within 0.1 eV in the total energy. The polarization energy was included throughout.

The results of the minimization are shown in Table III.3. To be aligned exactly along a $\langle 111 \rangle$ axis would require that $\theta = 54.74°$ or $\theta = 125.36°$, and that $\phi = 135°$ or $\phi = 45°$ depending on the [111] axis in question. The x, y and z components of the center of mass position, R_{com}, would all be equal to 1.08 (a.u.) with one ion at it's perfect lattice site and the other ion pointing towards an empty body-centered interstitial site (see Figure 2(b)–(e)). The energy of the initial $(V_k + e^-)$ configuration, with a pair of balanced tetrahedral bases, is also included for reference.

Table III.3
Ground state minimization results in the three configurations.
Energies in eV, positions in (a.u.), angles in degrees.
Further details can be found in the text.

	CaF_2	SrF_2
$(V_k + e^-)$		
E_{tot}	20.05	14.49
E_{elec}	7.44	2.96
R_{com}	(0.0, 2.58, 0.0)	(0.0, 2.90, 0.0)
θ, ϕ	90.0, 90.0	90.0, 90.0
configuration 1		
E_{tot}	9.45	7.81
E_{elec}	-5.66	-5.20
R_{com}	(1.18, -1.12, 1.13)	(1.10, -1.10, 1.11)
θ, ϕ	125.5, 135.7	125.4, 136.2
configuration 2		
E_{tot}	9.42	7.81
E_{elec}	-5.36	-5.26
R_{com}	(-1.12, 1.13, 1.14)	(-1.14, 1.14, 1.14)
θ, ϕ	55.5, 132.4	54.9, 133.6
configuration 3		
E_{tot}	9.45	7.80
E_{elec}	-5.57	-5.64
R_{com}	(-4.01, 1.17, 1.11)	(-4.67, 1.14, 1.09)
θ, ϕ	56.8, 44.2	56.7, 44.7

We can see that the total energy of all three configurations are almost equal to one another for both CaF_2 and SrF_2 . There is a moderate variation in the electron energies but no significant trends may be observed. In all cases, the molecule remained close to the $\langle 111 \rangle$ axis with the only noticeable change in position being a slight shift of R_{com} towards the BCI site.

The resulting distortion fields show fairly good symmetry characteristics. Each configuration contains a mirror plane ($C_{1'h}$ symmetry group) and in each case these ions were displaced more or less symmetrically with respect to this plane.

We can make a few general remarks about the distortion fields:

(i) The displacements in SrF_2 were larger than those in CaF_2 . This is mainly due to the larger lattice constant and smaller Born-Mayer repulsive constants in SrF_2 , in effect making the SrF_2 crystal "softer".

(ii) Cations that are nearest-neighbours of the F center but not of the H center, move approximately radially in towards the F center. This has the effect of stabilizing the F center. In a calculation by Bartram *et al*[24], the inward displacement of cations surrounding a pure F center was found to be 1.5% of d_{nn} in CaF_2 and 2.8% of d_{nn} in SrF_2 . We found values ranging from 3.6% to 5.2% of d_{nn} in CaF_2 and from 2.2% to 6.5% of d_{nn} in SrF_2 . The lower range of these distortions are probably closer to the pure F center values because they are from the distortion field of configuration 1 where the hole is farthest away from these cations.

(iii) The other nearest-neighbour cations, *ie.* close to both the F and H centers, have considerably larger displacements with values ranging from 4.7% to 7.8% of d_{nn} in CaF_2

and from 3.8% to 9.2% of d_{nn} in SrF_2 . The large displacements are not surprising since these ions feel the effects of both the F center and the H center. The direction of these displacements was generally away from H center ions and toward the F center.

(iv) Nearest-neighbour anions to the H center always move away from the molecule ions. Their displacements were anywhere up to 6.5% of d_{nn} in CaF_2 and to 7.4% of d_{nn} in SrF_2 . This distortion is consistent with the electrostatic repulsion of like charges.

(v) Other ions, *ie.* next-nearest-neighbours to the F and H centers, move considerably less than the nearest neighbours. Their distortion is probably below the "noise" level of the calculation.

A typical equilibrium distortion field (displacements of ions from their perfect lattice sites) is shown in Table III.4. This example is for CaF_2 in configuration 2. The F center is at (0,2,0) and the H center is along the $[\bar{1}11]$ axis with one ion at (0,0,0); (the unit cell has a cube edge of length 4). The mirror plane is the [101] plane. Symmetry partners are indicated in the table by the arrows; the H center ions are numbered 1 and 11. All displacements are in (a.u.) while the original lattice positions are in units of the unit cell cube edge.

Table III.4

Equilibrium distortion field of CaF_2 in configuration 2

Details may be found in the text

ION	DX	DY	DZ	ORIGINAL POSITIONS		
1	-0.07864	-0.01051	0.07521	0	0	0 → H
2	0.10806	0.25879	-0.00109	1	1	1
3	0.05491	0.25906	-0.07915	-1	1	-1
4	-0.12522	-0.15875	0.12547	-1	-1	1
5	0.05774	-0.05774	-0.05774	1	-1	-1
6	-0.14067	-0.11423	-0.10235	-2	0	0
7	0.01238	0.07510	0.07776	0	0	-2
8	0.00000	0.00000	0.00000	0	-2	0
9	-0.07446	0.00591	0.03640	2	0	0
10	0.14260	-0.11093	0.12625	0	0	2
11	-2.16264	-2.87887	2.19971	0	2	0 → H
12	-0.08078	0.06364	-0.06054	-2	2	0
13	-0.03113	-0.10746	0.07126	-2	0	2
14	0.10709	0.05023	0.15259	0	2	2
15	0.14190	0.03949	0.01461	2	2	0
16	0.03396	0.06278	-0.13388	0	2	-2
17	-0.12887	-0.08279	0.14464	1	3	-1
18	0.05931	-0.05525	0.02346	-1	1	3
19	0.13465	-0.12862	-0.12507	-1	3	1
20	-0.01581	-0.04743	0.00000	-3	1	1
21	0.03558	0.03721	0.02873	-2	2	2
22	0.00000	0.10000	0.00000	0	4	0

III.3 Absorption Energies

We now turn our attention to the absorption spectrum of the various STE (nearest neighbour F-H pair) configurations. We calculated the energies of the various first excited $2p$ states in all three configurations as well as the ground state energy to obtain the absorption spectrum.

For each configuration we used the distortion field of the ground state in accordance with the Franck-Condon principle.

There remains the question of basis optimization. In a system with high symmetry, such as an F center in cubic symmetry, the problem is merely that of optimizing the basis to get the lowest energy for a state of given symmetry. In the present problem however, we find that the symmetry is quite low especially because the H center is only approximately

along a $\langle 111 \rangle$ axis.

An s-like state is easy to represent. This is borne out in the fact that the energy of the ground state is relatively insensitive to variations in the actual floating bases used. A p-like state requires at least two gaussians and it is best to position these along the axis that the p state is expected to lie, separated by some distance.

The problem here is rather more complex, due to the fact that we have only qualitative ideas about the axes along which the p-like orbitals should be pointing. Furthermore, it is also not possible to determine *a priori* where the "nodal planes" should be placed. Because of this situation, we proceed as follows.

Eshita *et al*[12] have suggested that in each configuration the three p state axes are: (i) the p state perpendicular to the mirror plane, (ii) an axis contained in the mirror plane along the $\langle 100 \rangle$ cube edge direction and (iii) along the $\langle 110 \rangle$ axis contained in the mirror plane.

Along each of the appropriate axes, we optimized three pairs of gaussians symmetrically arranged about the vacancy. Each pair was placed at $\pm R$ with the same damping factor α. The combination of bases that gave the best results were $\alpha = 0.06(\text{a.u.})^{-2}$ and $\alpha = 0.10(\text{a.u.})^{-2}$ for CaF_2 and $\alpha = 0.06(\text{a.u.})^{-2}$ and $\alpha = 0.08(\text{a.u.})^{-2}$ in SrF_2 and we found that $R = 0.071(\text{a.u.})$ gave the best results for both CaF_2 and SrF_2 . The third pair of gaussians were placed at $R = 0.28(a.u.)$ with $\alpha = 0.04(\text{a.u.})^{-2}$. Addition of even more bases did give slightly lower energy, however the increase in computation time required did not justify the marginal improvement to the energy.

One point is worth mentioning here. When a pair of $1s$ gaussians, separated by $2R$

is used to represent a p-like orbital, the energies of the resulting even (s-like) and odd (p-like) states vary as a function of R for a given gaussian damping factor α. The even parity state energy is relatively stable. The odd parity energy will be close to that of the even parity state for very large R, because the splitting is small for large R. For very small R, numerical loss of precision makes the odd parity energy very unstable. This is a fairly well known phenomenon[46]. Therefore for a given α of a gaussian, there is a safe range of R. This is illustrated in Figure 3.

The absorption energies of all three F-H pair configurations have been studied using such separate sets of basis. The results are shown in Table III.5(a). It should be noted here that the three p-like states for a given configuration are only approximately orthogonal. The absorption energies are somewhat higher than the observed values. This is often the case in the one-electron Hartree-Fock calculations. Even for a single F center, the calculated energy for the $1s - 2p$ transition is higher by $\sim$1 eV than the experimental values. This problem is fairly well known and discussed by Harker[47] in some length. It is to be noted also that the crystal field splitting of the $1s - 2p$ absorption of the F-H pairs is fairly small and compatible with the observed absorption bandwidths which are in the 0.4–0.5eV range for both CaF_2 and SrF_2 .

In an attempt to get the s-like and the three p-like states mutually orthogonal we have obtained all the transition energies in a single secular determinant containing the three sets of basis described above plus an extra one at the vacancy. The results are presented in Tables III.5(b) and III.5(c). The s-like state energy has scarcely varied. Some of the p-like state energies have improved quite substantially, while the higher sublevel energies rise.

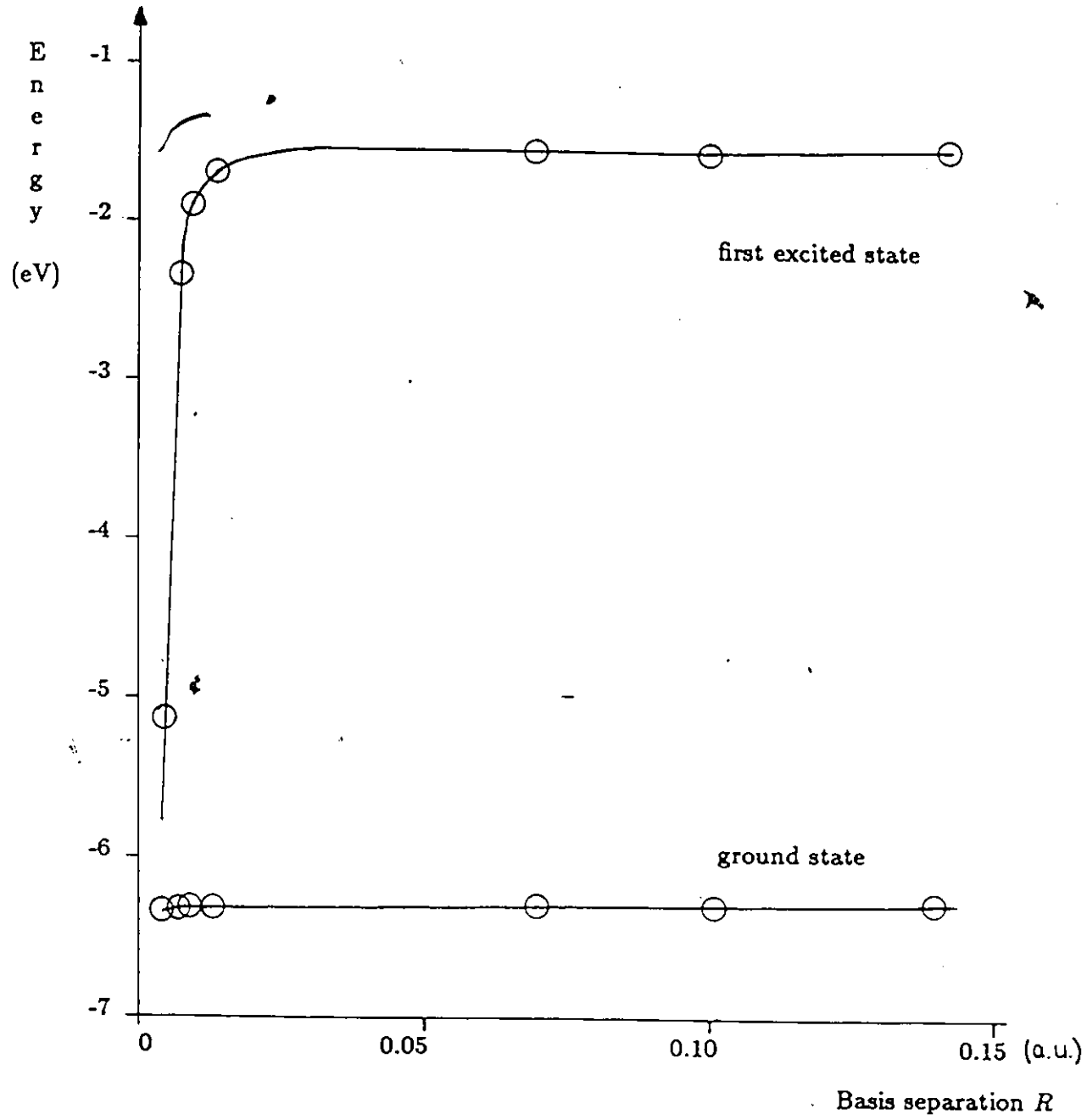

Figure 3

Variation of s-like and p-like state energies as a function of basis separation

Table III.5(a)

Absorption energies in the three configurations evaluated in each excited state separately (eV)

Excited state axis	Ground state E_{elec}	Ground state E_{pol}	Ground state $E_{elec}+E_{pol}$	p state E_{elec}	p state E_{pol}	p state $E_{elec}+E_{pol}$	ΔE
CaF_2							
Configuration 1							
$p[010] \sim \parallel$ mol.	-5.71	-0.31	-6.02	-0.11	-0.44	-0.55	5.47
$p[101] \sim$ towards mol.	-5.70	-0.31	-6.01	-0.05	-0.46	-0.51	5.50
$p[10\bar{1}] \perp$ plane	-5.70	-0.31	-6.01	+0.00	-0.51	-0.51	5.50
Configuration 2							
$p[10\bar{1}] \sim \parallel$ mol.	-5.44	-0.29	-5.73	+0.79	-0.48	+0.31	6.04
$p[101] \perp$ plane	-5.40	-0.30	-5.70	-0.28	-0.44	-0.72	4.98
$p[010] \sim$ towards mol.	-5.42	-0.29	-5.71	+0.60	-0.45	+0.15	5.86
Configuration 3							
$p[001] \sim$ towards mol.	-5.65	-0.30	-5.95	+0.05	-0.44	-0.39	5.56
$p[1\bar{1}0] \perp$ plane	-5.64	-0.30	-5.94	-0.14	-0.47	-0.61	5.33
$p[110] \sim \parallel$ mol.	-5.64	-0.30	-5.94	+0.36	-0.47	-0.11	5.83
SrF_2							
Configuration 1							
$p[010] \sim \parallel$ mol.	-5.26	-0.21	-5.47	-0.71	-0.28	-0.99	4.48
$p[101] \sim$ towards mol.	-5.25	-0.22	-5.47	-0.69	-0.32	-1.01	4.46
$p[10\bar{1}] \perp$ plane	-5.25	-0.22	-5.47	-0.51	-0.34	-0.85	4.62
Configuration 2							
$p[10\bar{1}] \sim \parallel$ mol.	-5.29	-0.21	-5.50	-0.26	-0.33	-0.59	4.91
$p[101] \perp$ plane	-5.27	-0.21	-5.48	-0.91	-0.34	-1.25	4.23
$p[010] \sim$ towards mol.	-5.29	-0.22	-5.51	-0.22	-0.32	-0.54	4.97
Configuration 3							
$p[001] \sim$ towards mol.	-5.67	-0.25	-5.92	-0.82	-0.34	-1.16	4.76
$p[1\bar{1}0] \perp$ plane	-5.67	-0.25	-5.92	-0.83	-0.38	-1.21	4.71
$p[110] \sim \parallel$ mol.	-5.67	-0.25	-5.92	-0.69	-0.36	-1.05	4.87

Table III.5(b)
Absorption energies for CaF_2 in the three configurations (eV).

State	E_{elec}	E_{pol}	$E_{elec}+E_{pol}$	ΔE	Exp't	ΔW
Configuration 1						
0 1*s* g.s.	-5.73	-0.31	-6.04		2.8	0.4
1 $p[010]$ ~‖ mol.	-0.52	-0.50	-1.02	5.02		
2 $p[101]$ ~ towards mol.	-0.05	-0.46	-0.51	5.53		
3 $p[10\bar{1}]$ ⊥ plane	+0.00	-0.51	-0.51	5.53		
Configuration 2						
0 1*s* g.s.	-5.49	-0.29	-5.78		2.8	0.4
1 $p[1\bar{2}\bar{1}]$ ~‖ mol.	-0.30	-0.46	-0.76	5.02		
2 $p[101]$ ⊥ plane	-0.28	-0.44	-0.72	5.06		
3 $p[\bar{1}\bar{1}1]$ ~ towards mol.	+1.26	-0.51	+0.75	6.53		
Configuration 3						
0 1*s* g.s.	-5.68	-0.30	-5.98		2.8	0.4
1 $p[001]$ ~ towards mol.	-0.38	-0.47	-0.85	5.13		
2 $p[1\bar{1}0]$ ⊥ plane	-0.14	-0.47	-0.61	5.37		
3 $p[110]$ ~‖ mol.	+0.41	-0.47	-0.06	5.92		
***F* center**						
0 1*s* g.s.	-3.63	-1.02	-4.65		3.3	0.4
1 2*p* degen.	+1.40	-1.05	+0.35	5.00		

This is to be expected to some extent, because the low symmetry of the system mixes some of the approximately orthogonal *p*-sublevels and results in a larger crystal field splitting. It is ultimately a problem of the size of the basis. We therefore suggest that the experimental absorption energies should be compared with the calculated energy difference between the *s*-like state and the lowest *p*-like state.

We see that the absorption peaks occur at a lower energy in SrF_2 as opposed to CaF_2 in agreement with experiment. Williams *et al*[10] have observed that the *F* absorption band in both crystals decompose with three distinct lifetime components. In CaF_2 , all three components have peaks at ≈2.8 eV, while SrF_2 shows more structure in the *F* band,

Table III.5(c)

Absorption energies for SrF_2 in the three configurations (eV).

State	E_{elec}	E_{pol}	$E_{elec} + E_{pol}$	ΔE	Exp't	ΔW
Configuration 1						
0 1s g.s.	-5.37	-0.21	-5.58		2.7	0.4
1 $p[010] \sim \parallel$ mol.	-1.35	-0.34	-1.69	3.89		
2 $p[101] \sim$ towards mol.	-0.69	-0.32	-1.01	4.57		
3 $p[10\bar{1}] \perp$ plane	-0.51	-0.34	-0.85	4.73		
Configuration 2						
0 1s g.s.	-5.41	-0.21	-5.62		2.4	0.4
1 $p[1\bar{2}\bar{1}] \sim \parallel$ mol.	-1.14	-0.32	-1.46	4.16		
2 $p[101] \perp$ plane	-0.91	-0.34	-1.25	4.37		
3 $p[\bar{1}\bar{1}1] \sim$ towards mol.	-0.04	-0.36	-0.40	5.21		
Configuration 3						
0 1s g.s.	-5.76	-0.25	-6.01		2.5	0.5
1 $p[110] \sim \parallel$ mol.	-1.45	-0.37	-1.82	4.19		
2 $p[1\bar{1}0] \perp$ plane	-0.83	-0.37	-1.20	4.81		
3 $p[001] \sim$ towards mol.	-0.71	-0.35	-1.06	4.95		
***F* center**						
0 1s g.s.	-4.46	-0.74	-5.20		2.85	0.3
1 2p degen.	+0.07	-0.84	-0.77	4.43		

decomposing at peaks of 2.4, 2.5 and 2.7 eV. It was not clear to Williams *et al* whether the different components are due to absorption of three different sublevels of the spin-triplet in one configuration or to a single unresolved triplet in three different configurations. Eshita *et al*[28] prefer the latter explanation and assigned each component to a specific configuration based on the relation of the lifetime of each state and the separation of the *F* and *H* centers.

The identification of the various excited state axes was made by plotting the amplitude of the wavefunction ϕ of each excited state in various planes. We have neglected the core orthogonalization part of the wavefunction. A sample of these plots is given in Figure 4.

This example is for CaF_2 in configuration 2 plotted in the [101] plane showing the four lowest electron states. A '9' in the diagram corresponds to the maximum amplitude of the wavefunction in this plane. The anion vacancy site is marked by an *.

Using this method we found that the p state axes agreed with Eshita *et al*'s[12] assignment in configurations 1 and 3, however configuration 2 had axes along [101] perpendicular to the mirror plane and along the $[\bar{1}\bar{1}1]$ and $[1\bar{2}\bar{1}]$ axes contained in the mirror plane. The absorption energies were recalculated in configuration 2 for both CaF_2 and SrF_2 using these axes as the p state axes with almost identical energies.

III.4 Interconversion barrier potentials

Eshita *et al*[12] showed that photo-excitation of the F center can induce motion of the V_k center, or inter-configuration conversion. They used cascade excitation spectroscopy and dichroism effects with SrF_2 to show that when one component of the F center absorption band is excited, the absorption of that component decreases while the others increase. Using their identification of the various components, they observed that conversion from configuration 2 to configuration 3 occured with an efficiency of 0.8 and the reverse conversion with an efficiency of 0.65. Conversion from configuration 2 to 1 also occured but with an efficiency $\frac{1}{10}$ of that from configuration 2 to 3. For this reason they did not study the latter process further. They also found that annihilation of configuration 2 resulted predominantly by excitation to the p orbital lying in the mirror plane along a $\langle 110 \rangle$ axis (*ie.* not the axis in the mirror plane along the cube edge $\langle 100 \rangle$). The reverse conversion resulted predominantly by excitation in the p orbital lying perpendicular to the mirror plane of configuration 3.

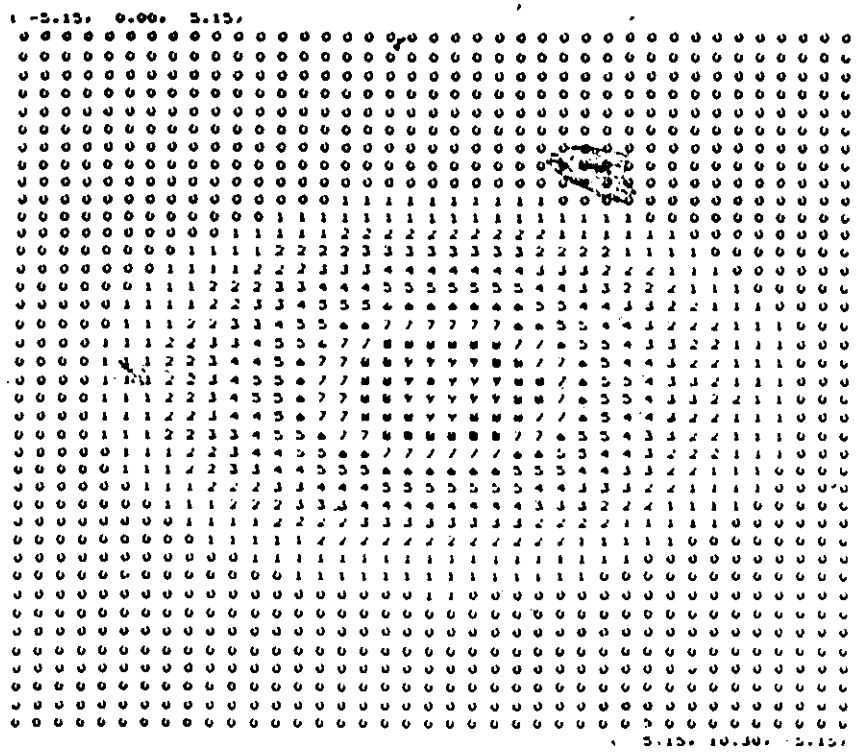

4(a)
Ground state
Max. ampl. 0.17
s-like

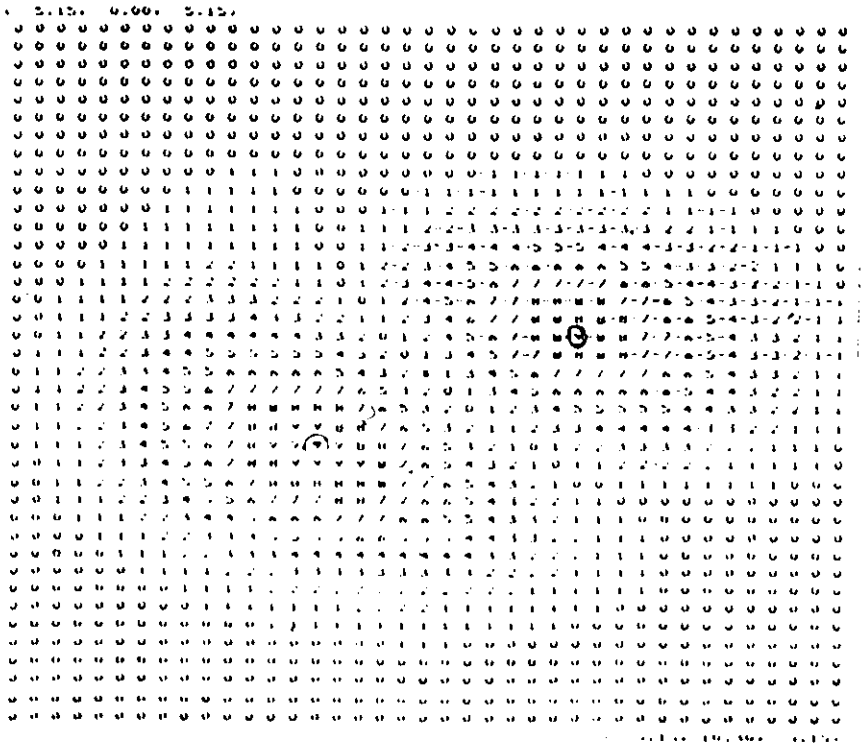

4(b)
1st excited state
Max. ampl. 0.15
p-like $\sim [1\bar{2}\bar{1}]$

Figure 4
Plot of ground and 1st excited state wavefunctions in the [101] plane.

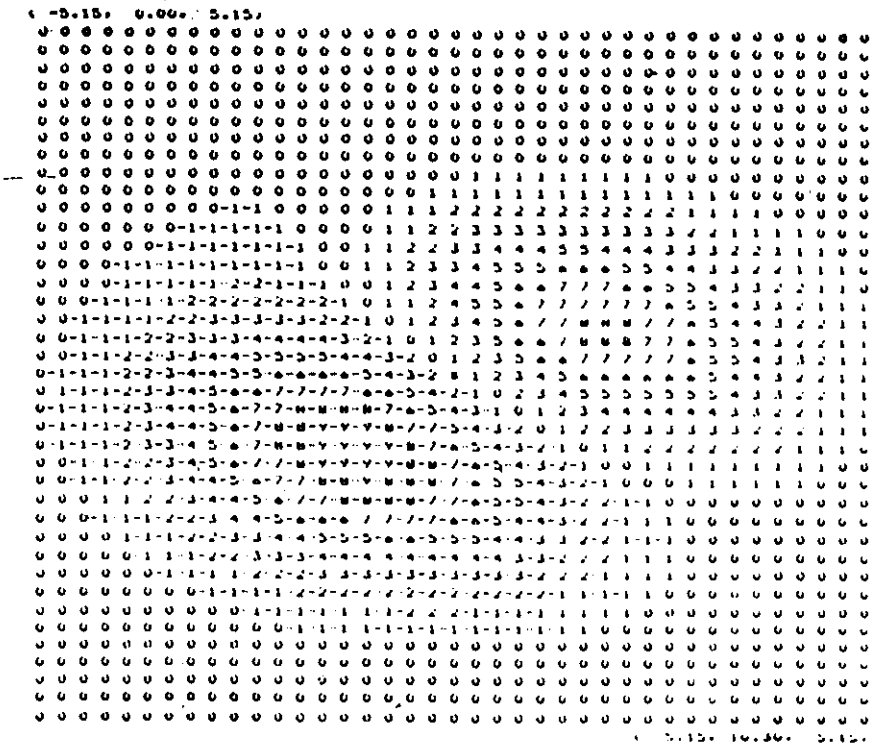

4(c)
2^{nd} excited state
Max. ampl. 0.08
(this is nodal plane)
p-like $\sim [101]$

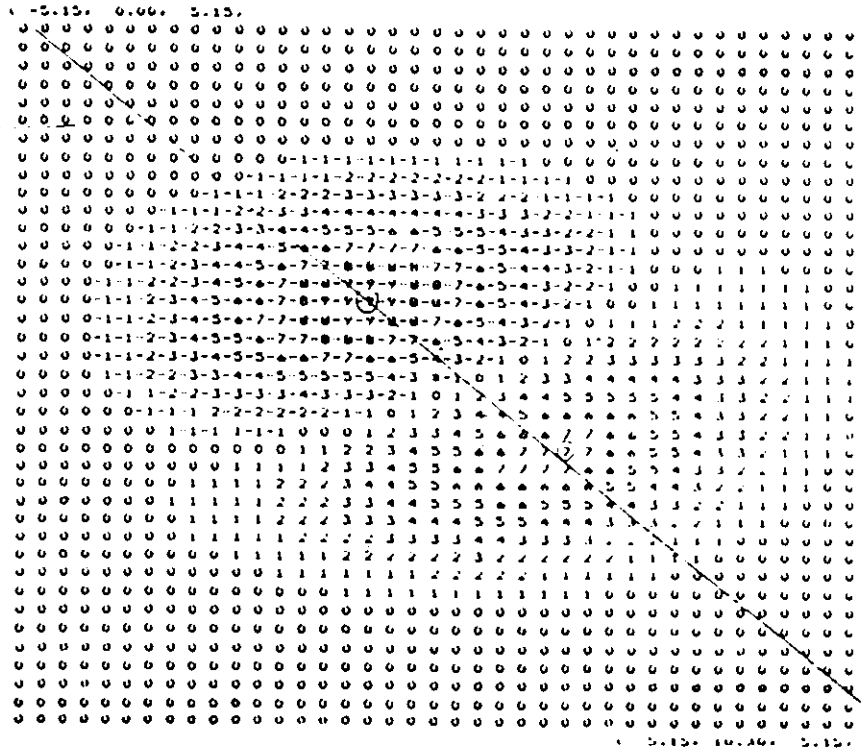

4(d)
3^{rd} excited state
Max. ampl. 0.20
p-like $\sim [\bar{1}\bar{1}1]$

Figure 4
Plot of 2^{nd} and 3^{rd} excited state wavefunctions in the [101] plane.

To verify the possibility of this effect we calculated the adiabatic potential curves for the four lowest states of the F center as the H center moves from configuration 2 to 3 (and vice versa) and between configurations 2 and 1 (and vice versa). We studied only the SrF_2 crystal since this is the only crystal on which experiments have been done.

We first defined a path along which the molecule was to move. We specified the coordinates of the molecule between two configurations, R_{com}, θ and ϕ, divided the path into several steps, placed the molecule at each step and minimized the total energy at each step by allowing the surrounding ions to relax. Details of the path will be given below.

Conversion between configurations 2 and 3 requires that the molecular bond be switched from one pair of anions to another. Therefore we could not treat this path in a continuous manner. To solve this problem we started from either configuration and moved the molecule to the midpoint of the path and stopped the calculation at this point. This gives rise to a small discontinuity in the potential curves.

In all our calculations, the F center is located at $(0,2,0)$ (the anion-anion distance is 2 units of the unit cell cube edge, refer to Figures 1 and 2; all positions below are in these units). In configuration 1, the H center is along the $[1\bar{1}1]$ axis with one ion at $(0,0,0)$ and the other at $(0.75,-0.75,0.75)$. Configuration 2 has the H center along $[\bar{1}11]$ with one ion at $(0,0,0)$ and the other at $(-0.75,0.75,0.75)$. Configuration 3 has the H center pointing in the $[111]$ direction, but with the substitutional anion at $(-2,0,0)$ and the interstitial ion at $(-1.25,0.75,0.75)$.

We defined the path from configuration 2 to 3 as follows: the interstitial ion moves in the $[100]$ direction from $x = -0.75$ to $x = -1.25$ in five steps. The other ion, the

substitutional anion, is placed at the proper V_k separation distance along the line joining the interstitial ion with the substitutional anion site of the appropriate configuration. This other ion is in effect being "dragged" along by the interstitial ion. The charge distribution of the H center remains constant throughout with a charge of -0.31 at the interstitial ion and -0.69 on the other ion of the molecule.

The path between configurations 1 and 2 was treated in a continuous way as follows. The center of mass position moves along the $\langle 111 \rangle$ axis of the appropriate configuration until it reaches the substitutional anion site at (0,0,0). It then switches to the $\langle 111 \rangle$ axis of the other configuration and moves to the equilibrium position in that configuration. During this time, the orientation of the molecule changes continuously between $\theta = 54.4°$ and $\theta = 125.6°$. On this path, ϕ remains constant at 135°. The charge distribution on the H center must change as well since the interstitial ion becomes the substitutional ion and vice versa. Therefore we made the hole distribution change continuously from one configuration to the other starting and ending with the equilibrium H center distribution of $Z = 0.69$. Therefore, at the midpoint of this path $R_{com} = (0,0,0)$, $\theta = 90°, \phi = 135°$ and the hole is shared equally by the two ions of the molecule.

The bases used for each calculation were the set of 6 optimized gaussians described in section III.3. Each p state was calculated separately with the p state axes along the appropriate directions for that configuration.

The positions of the surrounding lattice is minimized twice to obtain convergence to within 0.1 eV. At each step along the barrier, we used the distortion field of the previous step to start the calculation. At the first step, *ie.* at the ground state equilibrium

configuration, we used the distortion field of the ground state as a starting point for the minimization of all three excited states.

We should mention at this point that we tried a full minimization, *ie.* allowing the molecule's position to be minimized as well as the rest of the lattice ions, for the three excited states of configuration 2. Since bond switching is not treated, we expect that only spontaneous conversion to configuration 1 is possible. However, in all three cases the molecule remained in configuration 2. The fact that this did not occur does not preclude the possibility of conversion to this configuration since the molecule may have simply followed a path in the energy surface that contained an equilibrium position in configuration 2. It may also reflect the low efficiency of the conversion between configurations 1 and 2 observed by Eshita *et al.*

The potential curves we found are shown in Figures 5 and 6. The absorption energy, *ie.* the energy of the excited states calculated using the ground state distortion fields, are also shown in the diagrams.

Addressing first the conversion between configurations 2 and 3, we see that all four states have rather flat potential surfaces. The discontinuity at the midpoint arises partly because these configurations have different p state axes and partly because of the bond-switching problem mentioned above. Three possible paths for the molecule to follow upon excitation of the F center from the ground state are also shown. This shows that conversion is indeed possible between configurations 2 and 3 because enough energy is absorbed by the F center to overcome the potential energy barrier. In fact, the energy of the p orbital perpendicular to the mirror plane in configuration 3 decreases as the H center

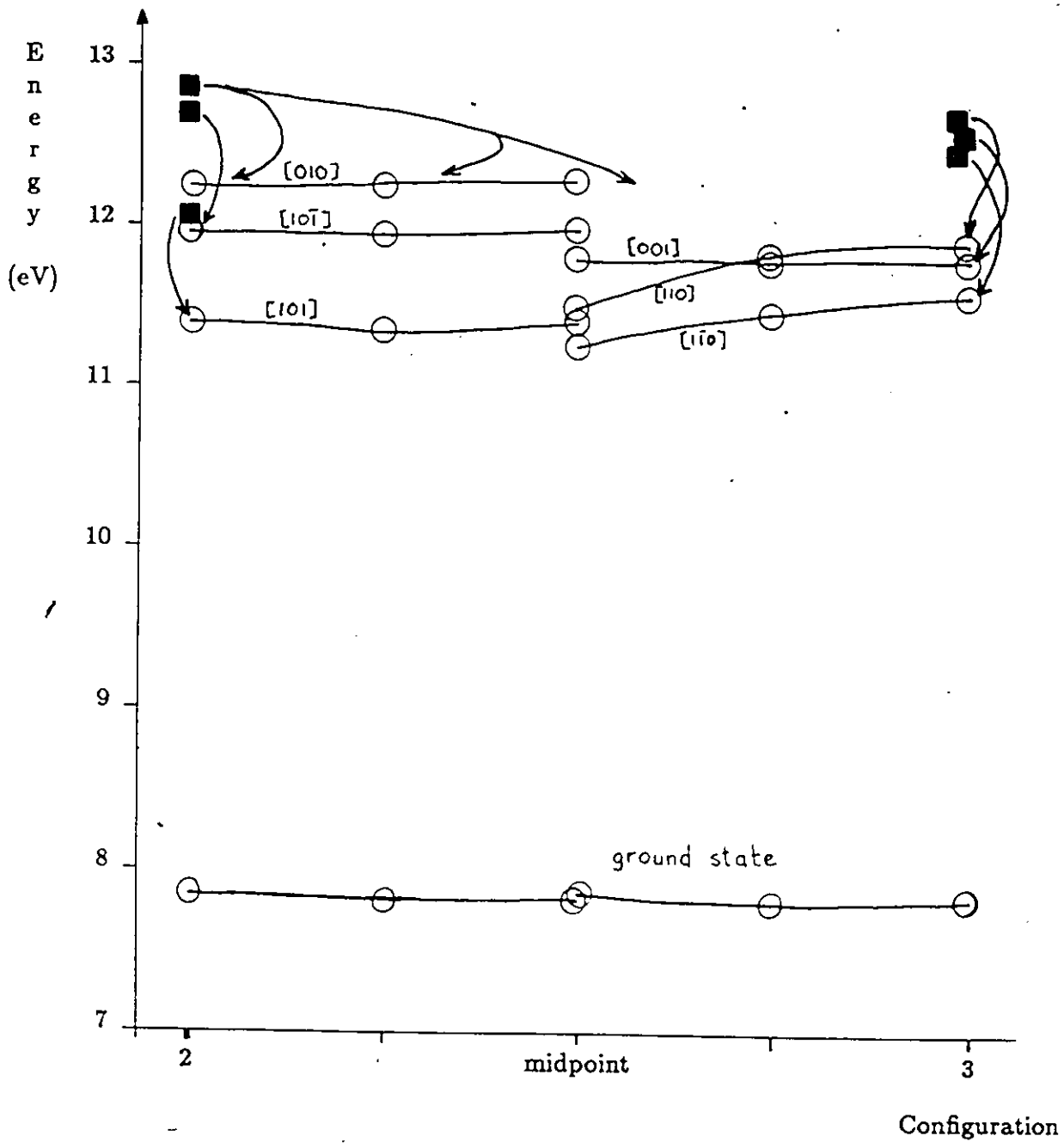

■ excited state energy using ground state distortion

Figure 5
Adiabatic potential curve between configurations 2 and 3 for SrF_2

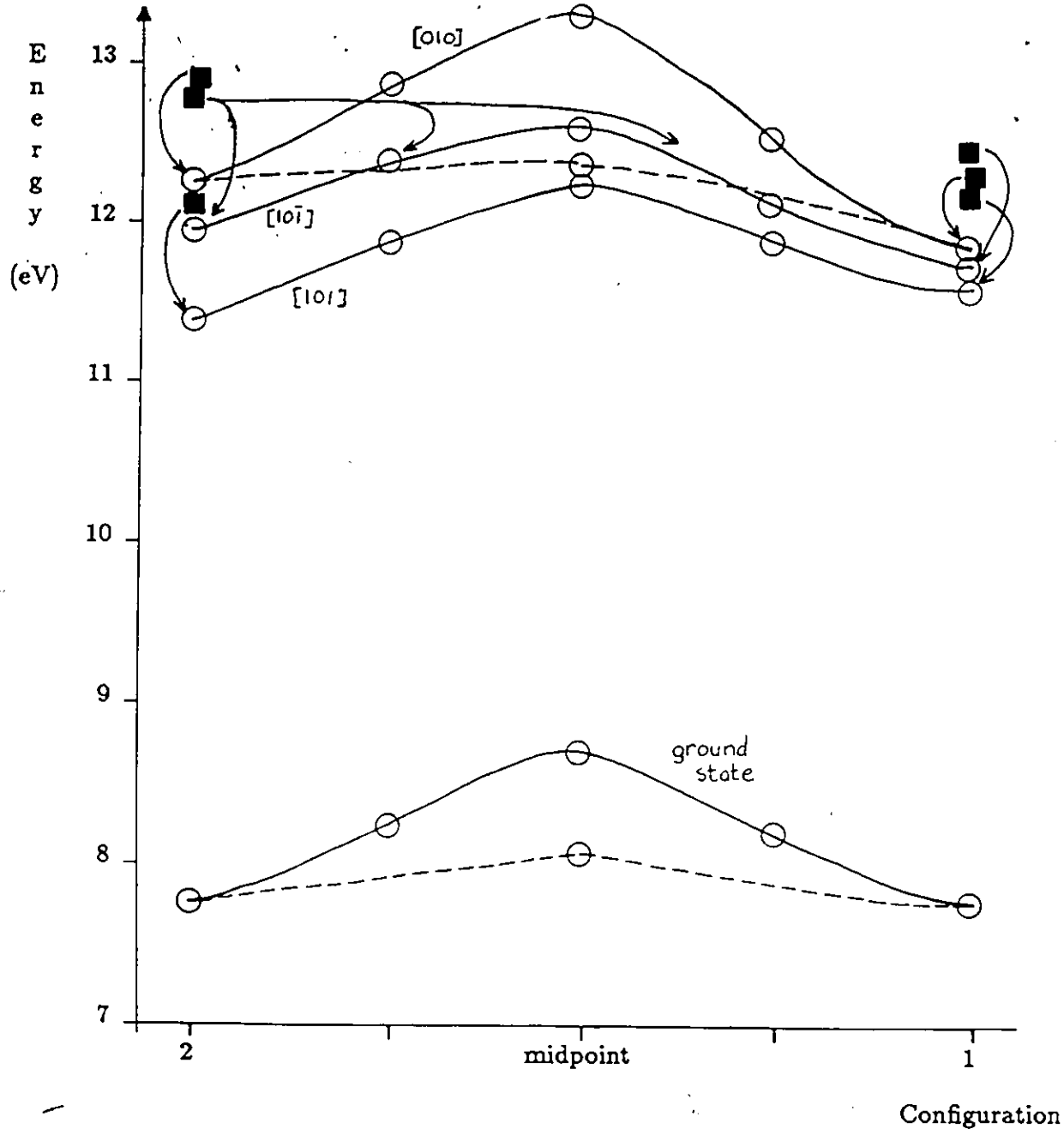

– – – – alternate path

■ excited state energy using ground state distortion

Figure 6
Adiabatic potential curve between configurations 2 and 1 for SrF_2

moves towards configuration 2. This is the same state that Eshita *et al* have observed to favour the interconversion from this configuration.

The degree of flatness in the ground state potential would seem to indicate that conversion occurs even without excitation into the excited states of the F center. This process would rely on thermal activation. This is consistent with the observations of Williams *et al*[10] that upon warming the crystal from 10K to 77K, the three absorption band component lifetimes collapse into one component with a single lifetime. This suggests that thermal equilibrium has been attained with one component feeding the other and vice versa.

Turning now to the conversion between configurations 1 and 2, we see some difference with the corresponding curves for configurations 2 and 3. We attribute this difference to an uncertainty in choosing the path for the molecule between the configurations. To show this we recalculated the energies of the ground state and the highest excited state shown (p in the [010] direction) at the midpoint using a different path. The results of this calculation are also shown on the graph. In this case we placed the molecule's center of mass at (0,0,0.4) instead of at (0,0,0) at the midpoint of the path. The lowering of the barrier (by $\sim$ 1 eV) makes sense intuitively because of the smaller short range repulsion on the new path, between the anions of the molecule and the cations at (1,-1,-1) and (-1,1,-1). There may also be some error in the charge distribution along our path because at the midpoint, one ion is considerably closer to the F center than the other, which would favour the hole more on one side rather than being shared equally.

We can therefore regard the potential barrier curves between configurations 1 and 2

and between configurations 2 and 3 as being essentially similar, with very small barriers for inter-configuration conversion in all states. The low conversion efficiency from configuration 2 to 1 simply reflects the greater distance to be travelled by the H center in this process as opposed to conversion between configurations 2 and 3.

CHAPTER IV - *Discussion and Conclusions*

The goal of this work was to study the structure of the STE in alkaline-earth fluorides. We found that at equilibrium, the STE resembles a pair of nearest or next-nearest neighbour F and H centers, as observed experimentally. We calculated the absorption spectrum of the F center in the various configurations of the STE and found this to be in reasonable agreement with experiment. We also showed that the observed interconversion between the various configurations is energetically possible.

The advantage of our method is the ease with which it may be applied to a defect system containing an excited electron. We treated the lattice distortions induced by the defect and the electron wavefunction in a self-consistent way. This has been shown to be crucial to this type of problem. The defect electron wavefunction is recalculated at each step by a hybrid pseudopotential scheme as the total energy of the system is minimized with respect to each ion position. The exclusive use of floating $1s$ gaussians for the electron basis set allows this calculation to be easily and efficiently carried out.

We have formulated a simple and efficient minimization scheme which is, at the same time, general enough to handle systems of low symmetry. Convergence is rapidly attained within a few iterations.

The lattice Coulomb energy, short range repulsive energy and polarization energy are also all calculated by numerically efficient techniques.

We have made a number of approximations, however, most of them related to the H center. The first of these is the "molecule in a lattice" model to represent the H center. This has been shown to be a valid approximation for a pure V_k or H center. However, the

effects of a nearby F center on an H center have not been included. This effect should be small since electrostatically, the F center resembles a fluoride ion. The effects of the lattice on an F_2^- molecule are included mainly through the Madelung potential on the two sites of the molecule and the electron can almost be regarded as a point charge in this respect.

We have represented the core of F_2^- with the molecular orbitals of Gilbert and Wahl for a free molecule. It is known from an analysis of H centers (Parker *et al*) that the hole charge is distributed unequally on the two fluorine cores. We do not know how to represent this in the hybrid pseudopotential approach. The unequal core structure, however, is understood to have a smaller effect on the electron state than the net charges on the two ions, for which we have used the values obtained for pure H centers. In the study of the inter-configuration conversion, the hole charge distribution undergoes some change which we have treated in an arbitrary, yet physically reasonable way.

We have used various interpolation formulae in the evaluation of the electron energy. We found that the RMS deviation of a least squares fit was less than 10^{-2} in all cases so that we expect that the error introduced into the electron energy due to these approximations to be on the order of 1%, which is small compared to the other approximations made. Yet this approximation is certainly an improvement over the Bartram, Stoneham and Gash approximation whereby the electron wavefunction is assumed to be slowly varying over the outer s and p orbitals of the ions.

There are various other approximations we have made including the neglect of the overlap of neighbouring ionic orbitals and various approximations in dealing with the

polarization energy. The neglect of overlap of core orbitals, especially for the anions, has to be addressed in order to improve on our method[47]. The various approximations for the polarization energy are acceptable because the defect system is electrically neutral. This could be improved by employing the shell model, for example.

A special problem we encountered is the low symmetry of the system. The H center is not exactly along the $\langle 111 \rangle$ axis due to the perturbation produced by the nearby F center. This has a subtle influence on the p-like excited states of the F center electron. While the s-like state can be simulated adequately by a suitable set of gaussian bases, there is some difficulty in producing good p-like states. We have only approximate ideas about the location of the nodal planes of the p states. A more precise determination of their location can be determined by more search.

The inadequacy of the one electron Hartree-Fock approximation can be seen in the absorption energies of the pure F center which are higher than the observed values. This is a generally observed trend in most one electron calculations[47]. An all out many electron Hartree-Fock calculations on defects in insulators is being attempted by other workers[48]. In view of the prohibitively high cost of such a computation (about 5000 sec of CPU for a simple F center in MgO with a CRAY supercomputer), it seems more practical to improve on the approximate methods such as the present one. It should be noted that all of the above approximations can contribute to the discrepancy of our calculated absorption energies with the observed spectrum.

One further improvement on our method could also be made by giving a better treatment of the molecule. Work is presently under way using a CNDO calculation for the

molecular orbitals that determines the hole charge distribution from the lattice potential and also allows bond switching to occur. This will allow a self-consistent study of the present system where the electron and the hole are influencing each other's state. A preliminary work using an extended Hückel treatment for the molecule was found to be inadequate. The CNDO method uses an iterative approach to deal with the lattice potentials and to determine the molecular orbitals. Bond switching will be very useful in examining the interconversion barrier potentials as we may be able to see spontaneous conversion between the configurations. We shall also be able to determine the transition energies of the hole states of the H center which will provide a useful comparison with experiment.

In summary, the main results of this work are: (i) the equilibrium configuration of the STE in the alkaline earth halides is like a nearest neighbour F-H center pair; (ii) the driving force for the large lattice distortion is the interaction of the defect electron with the lattice, which we have treated self-consistently; (iii) we have also shown that there is a good probability that conversion between configurations may take place and (iv) our calculated absorption energies are somewhat higher than the observed values mainly due to the one-electron Hartree-Fock approximation, yet they are in reasonable agreement with experiment in view of the approximations made. The principal results, namely the instability of the STE as a $(V_k + e^-)$ system and the interconversion between F-H pair configurations, were obtained consistently while we tried various levels of approximation, *eg.* the hole charge distribution, the ion-size treatment *vs.* the hybrid pseudopotential method and the treatment of the polarization energy.

APPENDIX A - *Properties of Gaussians*

We shall deal frequently with gaussians. What follows is a partial list of their properties. An excellent treatment of this subject may be found in reference (39).

The gaussian is defined as:

$$G_i(\vec{r}_i) = e^{-\alpha_i \vec{r}_i^{\,2}}, \qquad (\alpha_i > 0) \tag{A.1}$$

where the gaussian is centered at $\vec{R}_i$ and $\vec{r}_i = \vec{r} - \vec{R}_i$.

The product of two gaussians centered at any two sites, is itself a gaussian centered at a third site:

$$G_i(\vec{r}_i)G_j(\vec{r}_j) = KG_k(\vec{r}_k) \tag{A.2}$$

where

$$K = e^{-\left(\frac{\alpha_i \alpha_j}{\alpha_i + \alpha_j}|\vec{R}_i - \vec{R}_j|^2\right)} \tag{A.3}$$

$$\alpha_k = \alpha_i + \alpha_j \tag{A.4}$$

$$\text{and} \qquad \vec{R}_k = \frac{\alpha_i \vec{R}_i + \alpha_j \vec{R}_j}{\alpha_i + \alpha_j} \tag{A.5}$$

The integral of a gaussian in one dimension is:

$$\int_0^\infty t^n e^{-\alpha t^2}\, dt = \frac{1}{2}\alpha^{-\frac{(n+1)}{2}}\Gamma\left(\frac{(n+1)}{2}\right) \tag{A.6}$$

and in three dimensions it is:

$$\int e^{-\alpha_i \vec{r}_i^{\,2}}\, d\tau = \left(\frac{\pi}{\alpha_i}\right)^{\frac{3}{2}}. \tag{A.7}$$

For example,

$$\langle G_i(\vec{r}_i)|G_j(\vec{r}_j)\rangle = \left(\frac{\pi}{\alpha_i + \alpha_j}\right)^{\frac{3}{2}} e^{-\left(\frac{\alpha_i \alpha_j}{\alpha_i + \alpha_j}|\vec{R}_i - \vec{R}_j|^2\right)} \tag{A.8}$$

which is evaluated using equations (A.2) and (A.7).

Expressions involving an integration over one or more components of $\vec{r}$ and a gaussian can be derived from the fact that:

$$(x - X_i)e^{-\alpha_i \vec{r}_i{}^2} = \frac{1}{2\alpha_i} \frac{\partial}{\partial X_i} e^{-\alpha_i \vec{r}_i{}^2}. \qquad (A.9)$$

Further examples of integration involving gaussians are given in equations (B.10) and (B.11).

APPENDIX B - *Evaluation of the Hamiltonian*

B.1 Schrödinger equation

We start with the pseudo-wavefunction, ϕ_j, which is orthogonalized to all core orbitals, $\chi_{\gamma,\lambda}$:

$$|\psi_j\rangle = |\phi_j\rangle - \sum_{\gamma,\lambda} |\chi_{\gamma,\lambda}\rangle\langle\chi_{\gamma,\lambda}|\phi_j\rangle \tag{B.1}$$

and we must solve the eigenvalue problem:

$$\langle\psi_i|H|\psi_j\rangle = E\langle\psi_i|\psi_j\rangle \tag{B.2}$$

where,

$$\begin{aligned}\langle\psi_i|H|\psi_j\rangle = \langle\phi_i|H|\phi_j\rangle &- \sum_{\gamma,\lambda}\langle\phi_i|\chi_{\gamma,\lambda}\rangle\langle\chi_{\gamma,\lambda}|H|\phi_j\rangle \\ &- \sum_{\gamma,\lambda}\langle\chi_{\gamma,\lambda}|\phi_j\rangle\langle\phi_i|H|\chi_{\gamma,\lambda}\rangle + \sum_{\gamma,\lambda}\sum_{\gamma'\lambda'}\langle\chi_{\gamma'\lambda'}|\phi_j\rangle\langle\phi_i|\chi_{\gamma,\lambda}\rangle\langle\chi_{\gamma,\lambda}|H|\chi_{\gamma'\lambda'}\rangle\end{aligned} \tag{B.3}$$

where $H = T + V_{PI} + (V - V_{PI})$. For terms like $\langle\phi_i|H|\chi_{\gamma,\lambda}\rangle$ and $\langle\chi_{\gamma'\lambda'}|H|\chi_{\gamma,\lambda}\rangle$ we make the following approximation, assuming that there is no overlap between cores on different ions:

$$\langle\chi_{\gamma'\lambda'}|\chi_{\gamma,\lambda}\rangle = \delta_{\gamma\gamma'}\delta_{\lambda\lambda'} \tag{B.4}$$

and:

$$\begin{aligned}H|\chi_{\gamma,\lambda}\rangle &= (E^0_{\gamma,\lambda} + \Delta E_\gamma)|\chi_{\gamma,\lambda}\rangle \\ &= E_{\gamma,\lambda}|\chi_{\gamma,\lambda}\rangle\end{aligned} \tag{B.5}$$

where $E^0_{\gamma,\lambda}$ is the the free atomic core energy, and ΔE_γ is the shift in the potential due to the rest of the lattice. For the anions, whose valence electron orbitals are known to

undergo a compression in an ionic lattice, we have recalculated $\chi_{\gamma,\lambda}$ and $(E^0_{\gamma,\lambda} + \Delta E_\gamma)$ using a modified SCF code that incorporates the point-ion lattice potential. For the cations, the free ion wavefunctions of Clementi and Roetti[26] are used with a constant shift ΔE for the Madelung potential.

Therefore,

$$\langle\psi_i|H|\psi_j\rangle = \langle\phi_i|H|\phi_j\rangle - 2\sum_{\gamma,\lambda} E_{\gamma,\lambda}\langle\phi_i|\chi_{\gamma,\lambda}\rangle\langle\chi_{\gamma,\lambda}|\phi_j\rangle + \sum_{\gamma,\lambda}\sum_{\gamma'\lambda'}\langle\chi_{\gamma,\lambda}|\phi_j\rangle\langle\phi_i|\chi_{\gamma'\lambda'}\rangle E_{\gamma,\lambda}\delta_{\gamma\gamma'}\delta_{\lambda\lambda'} \quad (B.6)$$

$$= \langle\phi_i|H|\phi_j\rangle - \sum_{\gamma,\lambda} E_{\gamma,\lambda}\langle\phi_i|\chi_{\gamma,\lambda}\rangle\langle\chi_{\gamma,\lambda}|\phi_j\rangle \quad (B.7)$$

Similarly,

$$\langle\psi_i|\psi_j\rangle = \langle\phi_i|\phi_j\rangle - 2\sum_{\gamma,\lambda}\langle\phi_i|\chi_{\gamma,\lambda}\rangle\langle\chi_{\gamma,\lambda}|\phi_j\rangle + \sum_{\gamma,\lambda}\sum_{\gamma'\lambda'}\langle\chi_{\gamma,\lambda}|\phi_j\rangle\langle\phi_i|\chi_{\gamma'\lambda'}\rangle\delta_{\gamma\gamma'}\delta_{\lambda\lambda'} \quad (B.8)$$

$$= \langle\phi_i|\phi_j\rangle - \sum_{\gamma,\lambda}\langle\phi_i|\chi_{\gamma,\lambda}\rangle\langle\chi_{\gamma,\lambda}|\phi_j\rangle \quad (B.9)$$

as shown in section II.3

The kinetic energy term is:

$$\langle\phi_i|T|\phi_j\rangle = \int e^{-\alpha_i\vec{r}_i^{\,2}}(-\frac{1}{2}\nabla^2)e^{-\alpha_j\vec{r}_j^{\,2}}\,d\tau$$

$$= \frac{\alpha_i\alpha_j}{\alpha_i+\alpha_j}\left(3 - 2\frac{\alpha_i\alpha_j}{\alpha_i+\alpha_j}|\vec{R}_i - \vec{R}_j|^2\right)\left(\frac{\pi}{\alpha_i+\alpha_j}\right)^{\frac{3}{2}} e^{-\left(\frac{\alpha_i\alpha_j}{\alpha_i+\alpha_j}|\vec{R}_i-\vec{R}_j|^2\right)} \quad (B.10)$$

The point-ion potential, V_{PI}, is given by:

$$\langle\phi_i|\frac{Z_\gamma}{|\vec{r}-\vec{R}_\gamma|}|\phi_j\rangle = \sum_\gamma \int e^{-\alpha_i\vec{r}_i^{\,2}}\frac{Z_\gamma}{|\vec{r}-\vec{R}_\gamma|}e^{-\alpha_j\vec{r}_j^{\,2}}\,d\tau$$

$$= \sum_\gamma Z_\gamma\left[\frac{2\pi}{\alpha_i+\alpha_j}F_0\big((\alpha_i+\alpha_j)|\vec{R}_k - \vec{R}_\gamma|^2\big)e^{-\left(\frac{\alpha_i\alpha_j}{\alpha_i+\alpha_j}|\vec{R}_i-\vec{R}_j|^2\right)}\right] \quad (B.11)$$

where Z_γ is the net charge on ion γ, $\vec{R}_k$ is defined as in equation (A.5) and

$$F_0(t) = \frac{1}{2}\sqrt{\frac{\pi}{t}}\mathrm{erf}(\sqrt{t}). \tag{B.12}$$

For ions in their perfect lattice positions the sum of equation (B.11) is evaluated by the Ewald method[49]. For ions that have been displaced from their perfect lattice positions the point-ion potential is evaluated using equation (B.11) (without the sum over γ).

B.2 Ion-size terms

Assuming that ϕ_i is slowly varying, we can expand $\phi_i(\vec{r}_i)$ in a multipolar series:

$$\phi_i(\vec{r} - \vec{R}_i) = 2\pi \sum_l F_l(\vec{r}, \vec{R}_i) \sum_m \left[Y_l^m(\hat{r})^* Y_l^m(\hat{R}_i) \right] \tag{B.13}$$

then we can expand this in a Taylor's series about $\vec{R}_i$:

$$\phi_i(\vec{r} - \vec{R}_i) = 2\pi \sum_l \left\{ \sum_n F_l^{(n)}(0, \vec{R}_i) r^n \right\} \sum_m \left[Y_l^m(\hat{r})^* Y_l^m(\hat{R}_i) \right] \tag{B.14}$$

where,

$$F_l(\vec{r}, \vec{R}_i) = \int \phi(\vec{r} - \vec{R}_i) P_l(\cos\Omega)\, d(\cos\Omega) \tag{B.15}$$

and $F_l^{(n)}$ is the n^{th} derivative of F_l. Ω is the angle between $\vec{r}$ and $\vec{R}_i$ and $P_l(x)$ are the Legendre polynomials.

Using this expression for ϕ, we can put it into equations (2.16) and (2.17) for $T_\gamma^{(1)}$ and $T_\gamma^{(2)}$ to get:

$$f_1 = \frac{1}{4}|F_0(0, \vec{R}_i)|^2 \tag{B.16}$$

$$f_2 = \frac{1}{4}F_0(0, \vec{R}_i) F_0^{(2)}(0, \vec{R}_i) \tag{B.17}$$

$$f_3 = \frac{9}{4}|F_1^{(1)}(0, \vec{R}_i)|^2 \tag{B.18}$$

and,

$$A_\gamma = \int (V - V_{PI})_\gamma \, d\tau - \sum_\gamma E^0_{\gamma,\lambda} B_{\gamma,\lambda} \tag{B.19}$$

$$J'_\gamma = \int (V - V_{PI})_\gamma r^2 \, d\tau - \sum_\gamma E^0_{\gamma,\lambda} K'_{\gamma,\lambda} \tag{B.20}$$

$$J_\gamma = \int r\cos\theta (V - V_{PI})_\gamma r\cos\theta \, d\tau - \sum_\gamma E^0_{\gamma,\lambda} K_{\gamma,\lambda} \tag{B.21}$$

$$B_\gamma = \sum_\lambda B_{\gamma,\lambda} = \sum_\lambda \left(\int \chi_{\gamma,\lambda} \, d\tau \right)^2 \tag{B.22}$$

$$K'_\gamma = \sum_\lambda K'_{\gamma,\lambda} = \sum_\lambda \left(\int \chi_{\gamma,\lambda} \, d\tau \right) \left(\int \chi_{\gamma,\lambda} r^2 \, d\tau \right) \tag{B.23}$$

$$K_\gamma = \sum_\lambda K_{\gamma,\lambda} = \sum_\lambda \left(\int r\cos\theta \chi_{\gamma,\lambda} \, d\tau \right)^2 \tag{B.24}$$

and the short range potential is given by:

$$\begin{aligned}(V - V_{PI})_\gamma = &-\frac{Z_\gamma - \tilde{Z}_\gamma}{|\vec{r} - \vec{R}_\gamma|} - 2\int \frac{\sum_\lambda |\chi_{\gamma,\lambda}(\vec{r}')|^2}{|\vec{r} - \vec{r}'|} \, d\tau' \\ &- \sum_\lambda \int \frac{\chi_{\gamma,\lambda}(\vec{r}) \chi^*_{\gamma,\lambda}(\vec{r}')}{|\vec{r} - \vec{r}'|} P_{12} d\tau'\end{aligned} \tag{B.25}$$

where $\tilde{Z}_\gamma$ is the charge of the nucleus of ion γ and P_{12} is the permutation operator.

APPENDIX C - *Molecular Orbitals*

The molecular orbitals we shall use are given by:

$$\Psi_\lambda^{MO} = \frac{\chi_\lambda(\vec{r}_a) \pm \chi_\lambda(\vec{r}_b)}{\sqrt{2(1 \pm O_\lambda)}} \tag{C.1}$$

where χ_λ is an atomic orbital of symmetry λ and

$$O_\lambda = \langle \chi_\lambda(\vec{r}_a) | \chi_\lambda(\vec{r}_b) \rangle. \tag{C.2}$$

$\vec{r}_a$ is defined as $\vec{r}_a = \vec{r} - \vec{R}_a$ where the ions of the molecule are at $\vec{R}_a$ and $\vec{R}_b$.

These wavefunctions are orthonormal:

$$\langle \Psi_\lambda^{MO} | \Psi_{\lambda'}^{MO} \rangle = \delta_{\lambda\lambda'} \tag{C.3}$$

and

$$\begin{aligned} \langle \Psi_\lambda^{MO} | \Psi_\lambda^{MO} \rangle = \frac{1}{2(1 \pm O_\lambda)} \Big[& \langle \chi_\lambda(\vec{r}_a) | \chi_\lambda(\vec{r}_a) \rangle \pm \langle \chi_\lambda(\vec{r}_a) | \chi_\lambda(\vec{r}_b) \rangle \\ & \pm \langle \chi_\lambda(\vec{r}_b) | \chi_\lambda(\vec{r}_a) \rangle + \langle \chi_\lambda(\vec{r}_b) | \chi_\lambda(\vec{r}_b) \rangle \Big] \end{aligned} \tag{C.4}$$

$$= \frac{1}{2(1 \pm O_\lambda)} [2 \pm 2O_\lambda] = 1 \tag{C.5}$$

The atomic orbitals, χ_λ, can be fitted to a set of gaussians as in the case of individual ions and the appropriate substitutions made in the discussion that follows.

The charge density due to the molecular orbitals is given by:

$$\rho(\vec{r}) = |\Psi_\lambda^{MO}(\vec{r})|^2 \tag{C.6}$$

$$= \frac{1}{2(1 \pm O_\lambda)} \left[\chi_\lambda^2(\vec{r}_a) \pm 2\chi_\lambda(\vec{r}_a)\chi_\lambda(\vec{r}_b) + \chi_\lambda^2(\vec{r}_b) \right] \tag{C.7}$$

and the screened Coulomb potential will be given by:

$$V_{sc}^{MO}(\vec{r}') = \int \frac{\rho(\vec{r})}{|\vec{r}' - \vec{r}|}\, d\tau \tag{C.8}$$

$$= \frac{1}{2(1 \pm O_\lambda)} \Big[\int \frac{d\tau}{|\vec{r}' - \vec{r}|} \chi_\lambda^2(\vec{r}_a) + \int \frac{d\tau}{|\vec{r}' - \vec{r}|} \chi_\lambda^2(\vec{r}_b) \pm 2 \int \frac{d\tau}{|\vec{r}' - \vec{r}|} \chi_\lambda(\vec{r}_a)\chi_\lambda(\vec{r}_b) \Big]. \tag{C.9}$$

The first two terms are similar to the corresponding terms for isolated ions and can be fitted to the same form of interpolation formula. The third term is an extra cross term; therefore we fit the screened Coulomb potential to an interpolation formula of the form:

$$V_{sc}^{MO} = \frac{A_{sc} e^{-\beta_{sc}\vec{r}_a^2}}{|\vec{r}_a|} + \frac{A_{sc} e^{-\beta_{sc}\vec{r}_b^2}}{|\vec{r}_b|} + \frac{A'_{sc} e^{-\beta'_{sc}\vec{r}_{com}^2}}{|\vec{r}_{com}|} \tag{C.10}$$

where $\vec{R}_{com} = (\vec{R}_a + \vec{R}_b)/2$.

Similarly, for the exchange interaction we have:

$$V_{ex}^{MO} = \frac{|\Psi_\lambda^{MO}(\vec{r}_1)\rangle\langle\Psi_\lambda^{MO}(\vec{r}_2)|}{|\vec{r}_1 - \vec{r}_2|} \tag{C.11}$$

$$= \frac{1}{2(1 \pm O_\lambda)} \Big[\frac{\chi_\lambda(\vec{r}_1 - \vec{r}_a)\chi_\lambda^*(\vec{r}_2 - \vec{r}_a)}{|\vec{r}_1 - \vec{r}_2|} + \frac{\chi_\lambda(\vec{r}_1 - \vec{r}_b)\chi_\lambda^*(\vec{r}_2 - \vec{r}_b)}{|\vec{r}_1 - \vec{r}_2|} \pm \frac{\chi_\lambda(\vec{r}_1 - \vec{r}_a)\chi_\lambda^*(\vec{r}_2 - \vec{r}_b)}{|\vec{r}_1 - \vec{r}_2|} \pm \frac{\chi_\lambda(\vec{r}_1 - \vec{r}_b)\chi_\lambda^*(\vec{r}_2 - \vec{r}_a)}{|\vec{r}_1 - \vec{r}_2|} \Big]. \tag{C.12}$$

Again the first two terms are similar to the corresponding individual ion terms and may be fitted to the same type of interpolation formula. Therefore, in the same manner as for the screened Coulomb potential, we use an extra term at the center of mass of the molecule in the interpolation formula to account for the cross terms:

$$V_{ex}^{MO} = A_{ex} e^{-\beta_{ex}\vec{r}_a^2} + A_{ex} e^{-\beta_{ex}\vec{r}_b^2} + A'_{ex} e^{-\beta'_{ex}\vec{r}_{com}^2}. \tag{C.13}$$

References

(1) W. Hayes(ed.), Crystals With the Fluorite Structure, Clarendon Press, 1974

(2) J.H. Beaumont, W. Hayes, D.L. Kirk and G.P. Summers, Proc. Roy. Soc. London **A315**, 69, 1970

(3) A.N. Jette and T.P. Das, Phys. Rev. **186**, 919, 1969

(4) S. Parker, K.S. Song, C.R.A. Catlow and A.M. Stoneham, J. Phys. C: Solid State Phys. **14**, 4009, 1981

(5) M.J. Norgett and A.M. Stoneham, J. Phys. C: Solid State Phys. **6**, 229, 1973

(6) P.J. Call, W. Hayes and M.N. Kabler, J. Phys. C: Solid State Phys. 8, L60, 1975

(7) R.T. Williams and M.N. Kabler, Phys. Rev. B **9**, 1897, 1974

(8) C.H. Leung, G. Brunet and K.S. Song, J. Phys. C: Solid State Phys. **18**, 4459, 1985

(9) R.T. Williams, K.S. Song, W.L. Faust and C.H. Leung, Phys. Rev. B **33**, 7232, 1986

(10) R.T. Williams, M.N. Kabler, W. Hayes and J.P. Stott, Phys. Rev. B **14**, 725, 1976

(11) T. Eshita, K. Tanimura and N. Itoh, Nucl. Istrum. Methods **B1**, 452, 1984

(12) T. Eshita, K. Tanimura and N. Itoh, Phys. Stat. Sol. b**122**, 489, 1984

(13) M. Adair, C.H. Leung and K.S. Song, J. Phys. C: Solid State Phys. **18**, L909, 1985

(14) K.S. Song,L. Emery and C.H. Leung, unpublished

(15) N. Itoh, A.M. Stoneham and A.H. Harker, J. Phys. C: Solid State Phys. **10**, 4197, 1977

(16) C.H. Leung and K.S. Song, Physica **114B**, 323, 1982

(17) F.W. De Wette and B.R.A. Nijboer, Physica **23**, 309, 1957

(18) F.W. De Wette and B.R.A. Hijboer, Physica **24**, 1105, 1958

(19) J.R. Reitz, R.N. Seitz and R.W. Genberg, J. Phys. Chem. Solids **19**, 73, 1961

(20) L. Emery, M.Sc. Thesis, University of Ottawa, 1983

(21) K.S. Song, L. Emery, G. Brunet and C.H. Leung, Nucl. Instrum. Methods **B1**, 456, 1984

(22) L. Emery, C.H. Leung and K.S. Song, J. Phys. C: Solid State Phys. **15**, L361, 1982

(23) R.D. Zwicker, Phys. Rev. B **18**, 2004, 1978

(24) R.H. Bartram, A.M. Stoneham and P. Gash, Phys. Rev. **176**, 1014, 1968

(25) C. Muhlhausen and R.G. Gordon, Phys. Rev. B **24**, 2147, 1981

(26) E. Clementi and C. Roetti, Atomic Data and Nuclear Data Tables **14**, 1974

(27) A.H. Harker, Ph.D. Thesis, University of Oxford, 1974

(28) T.L. Gilbert and A.C. Wahl, J. Chem. Phys. **55**, 5247, 1971

(29) N.F. Mott and M.J. Littleton, Trans. Faraday Soc. **34**, 485, 1938

(30) C.H. Leung and K.S. Song, J. Phys. C: Solid State Phys. **12**, 3921, 1979

(31) K.S. Song and C.H. Leung, Solid State Commun. **36**, 237, 1980

(32) P.J. Call, W. Hayes, R. Huzimura and M.N. Kabler, J. Phys. C: Solid State Phys. 8, L56, 1975

(33) R.T. Williams, B.B. Craig and W.L. Faust, Phys. Rev. Letters **52**, 1709, 1984

(34) M.N. Kabler and R.T. Williams, Phys. Rev. B **18**, 1948, 1978

(35) M.J. Norgett and A.M. Stoneham, J. Phys. C: Solid State Phys. **6**, 238, 1973

(36) K. Tanimura and N. Itoh, J. Phys. Chem. Solids **45**, 323, 1984

(37) C.H. Leung, L. Emery and K.S. Song, Phys. Rev. B **28**, 3474, 1983

(38) J.H. Crawford and L.M. Slifkin (eds.), Point Defects in Solids, Plenum Press, 1972

(39) I. Shavitt, Methods in Computational Physics, vol. 2, 1, 1963

(40) J. Callaway, Quantum Theory of the Solid State, part A, Academic Press, 1974

(41) M. Abramowitz and I.A. Stegun, Handbook of Mathematical Functions, Dover Publications, 1970

(42) K.S. Song, C.H. Leung and L. Emery, J. Phys. C: Solid State Phys. **17**, 3551, 1984

(43) J.R. Tessman, A.H. Kahn and W. Shockley, Phys. Rev. **92**, 890, 1953

(44) C.H. Leung and K.S. Song, Can. J. Phys. **58**, 412, 1980

(45) W. Känzig and T.O. Woodruff, J. Phys. Chem. Solids **9**, 70, 1958

(46) R.N. Euwena, D.L. Wilhite and G.T. Surratt, Phys. Rev. B **7**, 818, 1973

(47) A.H. Harker, Lecture Notes in Physics **166**, 82, 1982

(48) J.M. Vail and R. Pandey, Fifth Europhysical Topical Conference on Lattice Defects in Ionic Crystals, Spain, 1986

(49) M.P. Tosi, in Solid State Physics vol. 16, F. Seitz and D. Turnbull (eds.), Academic Press, 1, 1967

(50) B.C. Cavenett, W. Hayes, I.C. Hunter and A.M. Stoneham, Proc. Roy. Soc. London **A309**, 53, 1969